environmental microbiology

Environmental Microbiology (2022) **24**(9), 4030–4048 doi:10.1111/1462-2920.16087

Organic matter availability drives the spatial variation in the community composition and activity of Antarctic marine bacterioplankton

Judith Piontek,[1*] **Christian Meeske**,[1] **Christiane Hassenrück**,[1] **Anja Engel**[2] **and Klaus Jürgens**[1]

[1]*Leibniz Institute for Baltic Sea Research, Warnemünde, Germany.*

[2]*GEOMAR Helmholtz Centre for Ocean Research Kiel, Kiel, Germany.*

Summary

Carbon cycling by Antarctic microbial plankton is poorly understood but it plays a major role in CO_2 sequestration in the Southern Ocean. We investigated the summer bacterioplankton community in the largely understudied Weddell Sea, applying Illumina amplicon sequencing, measurements of bacterial production and chemical analyses of organic matter. The results revealed that the patchy distribution of productive coastal polynyas and less productive, mostly ice-covered sites was the major driver of the spatial changes in the taxonomic composition and activity of bacterioplankton. Gradients in organic matter availability induced by phytoplankton blooms were reflected in the concentrations and composition of dissolved carbohydrates and proteins. Bacterial production at bloom stations was, on average, 2.7 times higher than at less productive sites. Abundant bloom-responsive lineages were predominately affiliated with ubiquitous marine taxa, including *Polaribacter*, *Yoonia-Loktanella*, *Sulfitobacter*, the SAR92 clade, and *Ulvibacter*, suggesting a widespread genetic potential for adaptation to sub-zero seawater temperatures. A co-occurrence network analysis showed that dominant taxa at stations with low phytoplankton productivity were highly connected, indicating beneficial interactions. Overall, our study demonstrates that heterotrophic bacterial communities along Weddell Sea ice shelves were primarily constrained by the availability of labile organic matter rather than low seawater temperature.

Received 12 January, 2022; accepted 27 May, 2022. *For correspondence. E-mail judith.piontek@io-warnemuende.de; Tel. +49 38 51973491; Fax +49 381 5197211.

Introduction

Antarctic marginal seas are among the least studied cold oceans on Earth. Despite their negative temperatures, in summer they host productive phytoplankton blooms dominated by diatoms and the prymnesiophyte *Phaeocystis antarctica*. Roughly 30% of primary production in the Southern Ocean is exported out of the euphotic zone, a proportion that substantially exceeds the export efficiency in the temperate ocean (Henson *et al*., 2012). The locally high level of primary production together with the high rate of particle export in Antarctic shelf waters is an important contribution to the Southern Ocean's potential to act as a strong sink for anthropogenic carbon (Frölicher *et al*., 2015).

Spatial and temporal patterns in bacterial carbon remineralization at low seawater temperature are less well understood. Several studies have reported lower ratios of heterotrophic bacterial biomass production to primary production in high-latitude marine systems than in the temperate ocean, implying that efficient carbon sequestration is enhanced by a disproportionally low bacterial carbon re-mineralization at low seawater temperature (Pomeroy and Deibel, 1986; Morán *et al*., 2006; Ducklow *et al*., 2012). However, this notion of suppressed bacterial activity at sub-zero temperature is challenged by field surveys showing that maximum bacterial growth rates in Arctic and Antarctic marine systems overlap with the rates determined in the temperate ocean (Kirchman *et al*., 2009). Furthermore, a growing number of experimental studies demonstrated high activity of natural polar bacterioplankton at *in situ* temperatures after the addition of labile organic matter, suggesting that a low seawater temperature *per se* does not have an inhibitory effect (Kirchman *et al*., 2009; Ducklow *et al*., 2011; Sipler and Connelly, 2015; Manna *et al*., 2020). Based on these observations, strong bottom-up control of heterotrophic bacteria by limited availability of dissolved organic matter (DOM) has been proposed as an alternative explanation

for the low growth rates in polar oceans (Kirchman *et al*., 2009).

This study aims to explore the importance of organic matter availability for the activity and taxonomic composition of bacterioplankton along the eastern and southern shelves of the Weddell Sea. Sampling stations included two coastal polynyas, the Halley Bay Polynya and the Ronne Polynya, as well as stations outside the polynyas that were mostly ice-covered and/or further offshore. Coastal polynyas, seasonally recurring open waters surrounded by sea ice, are hotspots of biological activity (Arrigo and van Dijken, 2003). With an average annual production of 14 Tg C yr^{-1}, the Ronne Polynya is the second most productive coastal polynya system in the Southern Ocean (Arrigo and van Dijken, 2003). The natural gradient in phytoplankton standing stocks along the Weddell Sea shelves, encompassing a 50-fold change in depth-integrated chlorophyll *a* concentration at similar seawater temperatures of −1.8°C to −0.2°C, enabled a detailed investigation of the role of fresh organic matter in the phytoplankton-bacteria coupling. The major objectives were (i) to analyse the concentration and composition of DOM and (ii) to compare the structure and phylogenetic composition of bacterioplankton in productive polynyas and at less productive sites. The results allowed us to explore the significance of organic matter availability in the environmental control of heterotrophic bacterial activity at low seawater temperatures.

Experimental procedures

Sampling

Samples were collected at 25 stations during cruise PS111 of the RV *Polarstern*, from 26 January 2018 to 01 March 2018. The stations were located between 64°S and 78°S and between 5°E and 60°W in the southern Weddell Sea. At each station, seawater was sampled at five or six depths in the upper 100 m of the water column using a rosette sampler equipped with 24 Niskin bottles. A CTD system was used to determine the continuous depth profiles of temperature and salinity. A sensor for Chl-*a* fluorescence (Wet Labs ECO-AFL/FL, Sea Bird Scientific) was mounted on the sampler. The data on seawater temperature, salinity and fluorescence obtained in this study can be retrieved from the PANGAEA database (Janout *et al*., 2018; https://doi.org/10.1594/PANGAEA.895808).

Chlorophyll a

For the analysis of Chl-*a*, 1 L of seawater was filtered onto glass fibre filters (GF/F, Whatman) and stored at −80°C. Pigments were extracted in 96% ethanol and Chl-*a* concentrations were measured with a 10-AU Turner fluorometer (Turner Designs) (Welschmeyer, 1994). The values were integrated to 100 m depth (mg Chl-*a* m^{-2}).

Concentration and depletion of macronutrients

Dissolved inorganic phosphate, dissolved inorganic silicate, and nitrate and nitrite concentrations were determined with an auto-analyser (QuAAtro, Seal analytical) using standard colorimetric methods (Grasshoff *et al*., 1983).

Net community production (NCP) was estimated based on nitrate depletion in the upper 100 m of the water column. Nitrate concentrations were measured at five or six depths ($NO_{3\ measured}$, µmol L^{-1}) and integrated over depth. Assuming that nitrate concentrations at 100 m depth ($NO_{3\ 100m}$, µmol L^{-1}) were equivalent to pre-bloom concentrations, nitrate depletion (ΔNO_3, mmol NO_3 m^{-2}) could then be calculated as shown in Eq. 1:

$$\Delta NO_3 = \int_{100}^{0} NO_{3\,100m} - \int_{100}^{0} NO_{3\,measured} \quad (1)$$

The drawdown of nitrate was calculated only for stations where NO_3^- concentrations at and below 80 m depth were consistently 29.1–32.4 µmol L^{-1}. Nitrate concentrations in this range have been reported for winter water and/or pre-bloom situations in the Weddell Sea, the Ross Sea and the Amundsen Sea (Carlson *et al*., 2000; Smith *et al*., 2003; Lechtenfeld *et al*., 2014; Yager *et al*., 2016). The estimated depletions were considered as time-integrated changes over summer, since our sampling took place at the end of the productive season. Nitrate depletion was converted into seasonal NCP (mol C m^{-2} yr^{-1}) by applying a C:N ratio of 6.6 (Redfield, 1958), which has been validated for nutrient consumption in the Weddell Sea (Hoppema *et al*., 2007).

Dissolved organic matter

For the analysis of dissolved organic carbon (DOC) and total dissolved nitrogen, 20 ml of seawater was filtered through pre-combusted glass fibre filters (GF/F, Whatman) into pre-combusted glass ampoules (450°C for 8 h). The samples were acidified by the addition of 20 µl of 30% hydrochloric acid. The ampoules were then sealed by flaming and stored at 0–4°C until analysed using the high-temperature catalytic oxidation method (TOC-VCSH, Shimadzu) (Qian and Mopper, 1996; Engel and Galgani, 2016). Samples for the analysis of dissolved carbohydrates and amino acids were filtered through a 0.45-µm syringe filter (Acrodisk, Pall Corporation) into pre-combusted glass vials (450°C for 8 h) and stored at

−20°C. Combined carbohydrates were analysed by high-performance anion-exchange chromatography coupled with pulsed amperometric detection (ICS 3000, Dionex) using a CarboPac PA10 analytical column (Dionex). Prior to their analysis, the samples were desalinated using a dialysis membrane with a 1-kDa molecular weight cut-off (Spectra Por, Spectrum). This desalination procedure excludes carbohydrates with a molecular weight <1 kDa. Consequently, the analysed pool represented dissolved combined carbohydrates (DCCHO) >1 kDa. After desalination, the samples were hydrolyzed with 1 M hydrochloric acid and then neutralized by acid evaporation under a dinitrogen atmosphere and the addition of ultrapure water. A detailed description is given in Engel and Händel (2011). Concentrations of the neutral sugars fucose, rhamnose, arabinose, galactose, glucose and mannose/xylose were determined. Mannose and xylose co-eluted and were therefore quantified as a mixture. In addition to neutral sugars, the concentrations of the amino sugars glucosamine and galactosamine and of the acidic sugars glucuronic acid and galacturonic acid were analysed. The sum of the DCCHO, including the concentrations of all neutral sugars, amino sugars and acidic sugars, is reported in monomer equivalents per litre. The carbon-normalized yield of DCCHO [%DOC] was calculated as shown in Eq. 2:

$$\text{DCCHO}\,[\%\text{DOC}] = \text{DCCHO-C}/\text{DOC} \times 100 \quad (2)$$

where DCCHO-C is the summed carbon concentration of DCCHO, calculated by multiplying the monomer concentration of each sugar by the respective number of carbon atoms and then summing the results.

Dissolved amino acids (DAA) were analysed by high-performance liquid chromatography (HPLC), after hydrolysis with 6 M hydrochloric acid at 100°C for 20 h, followed by neutralization and derivatization with ortho-phthaldialdehyde (Lindroth and Mopper, 1979). The HPLC system (Agilent 1260) was equipped with a C18 column (Phenomenex Kinetex). Concentrations of aspartic acid, glutamic acid, serine, glycine, threonine, arginine, alanine, γ-aminobutyric acid, tyrosine, valine, isoleucine, phenylalanine and leucine were determined. The summed concentration of all individual amino acids is reported in monomer equivalents per litre.

The carbon-normalized yield of DAA [%DOC] was calculated according to Eq. 3:

$$\text{DAA}\,[\%\text{DOC}] = \text{DAA-C}/\text{DOC} \times 100 \quad (3)$$

where DAA-C is the summed carbon concentration of DAA, calculated by multiplying the monomer concentration of each amino acid by the respective number of carbon atoms and then summing the results.

Abundance of prokaryotes

Seawater samples for the analysis of prokaryotic cell numbers were fixed on board by an 1-h incubation with 1% paraformaldehyde and 0.05% glutaraldehyde (final concentrations) at 5°C in the dark. The samples were stored at −80°C until their analysis by flow cytometry (FACSCalibur, Becton Dickinson). The cells were counted after staining with the DNA-binding dye SYBR Green I (Invitrogen). Cell numbers were estimated after visual inspection and manual gating of the population in the cytogram of side scatter versus green fluorescence, using the software CellQuest Pro (Becton Dickinson). Yellow-green latex beads (0.5 μm, Polysciences) served as the internal standard.

For the enumeration of nanoflagellates, 10 ml of seawater was fixed with 2% formaldehyde (final concentration) and filtered onto black 0.2 μm-polycarbonate filters. The filters were stored at −20°C. Nanoflagellates were stained with 4′,6-diamidino-2-phenylindole and then counted at 630× magnification using an epifluorescence microscope (Axioskop 2 MOT Plus, Zeiss).

Bacterial biomass production

Bacterial biomass production was estimated based on the incorporation of [^{3}H]-leucine, as described by Simon and Azam (1989). Three 10-ml aliquots of unfiltered seawater were incubated for 2 h at 0°C with [^{3}H]-leucine (specific activity 102.3 Ci mmol^{-1}) at a final concentration of 20 nmol L^{-1}. The incubations were terminated by the addition of 1% formaldehyde (final concentration). Blanks were prepared from samples fixed with 1% formaldehyde (final concentration) prior to the addition of the radioactive tracer. After the incubation, the samples and blanks were filtered onto 0.2-μm polycarbonate filters and rinsed with 10 ml of cold 5% trichloroacetic acid. The filters were dissolved in 4 ml of scintillation cocktail (Ultima Gold F, Perkin Elmer) and the amount of incorporated [^{3}H]-leucine was analysed using a liquid scintillation counter (Tri-Carb, Packard). Bacterial biomass production was estimated using a conversion factor of 1.5 kg C mol leucine^{-1}, assuming no intracellular isotope dilution (Simon and Azam, 1989).

Nucleic acid extraction, high-throughput amplicon sequencing and sequence analysis

One litre of each seawater sample was filtered onto a 0.2 μm-polycarbonate filter for the extraction of nucleic acids and subsequent sequencing of 16S rRNA genes and transcripts. The filters were flash-frozen in liquid nitrogen and stored at −80°C. Nucleic acids were extracted using the AllPrep DNA/RNA mini kit (Qiagen),

which allows the simultaneous purification of genomic DNA and total RNA from the same sample. Contaminating DNA in the RNA fraction was removed using the Turbo DNA-free kit (Invitrogen). The RNA of each sample was transcribed into cDNA using the universal primer 1492R (5′-GGTTACCTTGTTACGACTT-3′) (Lane, 1991) and the MultiScribe Reverse Transcriptase (Invitrogen). The cDNA of all samples was checked for contaminating DNA by PCR with the primer pair Com1 and Com2-Ph (Schwieger and Tebbe, 1998). The samples were sent to LGC Genomics GmbH (Berlin) for 16S rRNA amplicon sequencing, in which the hypervariable V3–V4 region of the 16S rRNA sequence was amplified in the DNA extracts and in the cDNA of all samples using the universal prokaryotic primers U341F (5′-CCTAYGGGRBGCAS CAG-3′) and U806R (5′-GGACTACNNGGGTATCTAAT-3′) (Sundberg *et al*., 2013). The PCRs included 1–10 ng each of the DNA extract and cDNA (total volume 1 μl), 15 pmol of each forward and reverse primer in 20 μl of 1× MyTaq buffer containing 1.5 units of MyTaq DNA polymerase (Bioline) and 2 μl of BioStabII PCR Enhancer (Sigma). For each sample, the forward and reverse primers had the same 10-nucleotide barcode sequence. The PCRs were carried out for 30 cycles using the following parameters: 1 min 96°C pre-denaturation, 96°C for 15 s, 50°C for 30 s, 70°C for 90 s. Concentrations of the 16S amplicon were determined by gel electrophoresis. Twenty nanogram of amplicon DNA from each sample was pooled for up to 48 samples carrying different barcodes. The amplicon pools were purified with one volume of AMPure XP beads (Agencourt) to remove primer dimers and other small mispriming products, followed by an additional purification on MiniElute columns (Qiagen). Illumina libraries were constructed using 100 ng of each purified amplicon pool DNA and the Ovation Rapid DR multiplex system 1–96 (NuGEN). The libraries were pooled and size selected during preparative gel electrophoresis. Sequencing was performed on an Illumina MiSeq using the V3 Chemistry (Illumina) with paired-end reads of 2 × 300 bp.

After sequencing, primer sequences from the demultiplexed raw paired-end fastq files were cut and the data were further processed using the package dada2 in R (Callahan *et al*., 2016). The dada2 pipeline infers exact amplicon sequence variants (ASVs) instead of building operational taxonomic units based on sequence similarity thresholds (Callahan *et al*., 2017). Taxonomic assignment was determined by aligning the sequences with those in the silva_nr_v138 database (Quast *et al*., 2013). Sequences classified as chloroplasts were extracted and assigned using the PhytoREF database (PR2 version 4.12.0) to explore the taxonomic composition of phytoplankton (Decelle *et al*., 2015).

Data analysis and statistical tests

Chemical and amplicon sequencing data were analysed and statistical testing was performed using R in RStudio (RStudio Team, 2020; R Core Team, 2021).

A principal component analysis (PCA) of the DCCHO and DAA composition in surface waters was conducted using the R packages vegan (Oksanen *et al*., 2020). Differences in the DOM concentrations between Bloom stations and Low-Chl stations and between the upper mixed layer (0–35 m) and depth intervals below the pycnocline (40–100 m) were tested for significance in a two-way ANOVA.

The alpha-diversity of the bacterial communities was investigated using diversity indices. The Chao1 and Shannon indices were calculated using the R package iNEXT (Hsieh *et al*., 2020). Differences in diversity indices between Bloom stations and Low-Chl stations and between the upper mixed layer (0–35 m) and depth intervals below the pycnocline (40–100 m) were tested for significance in a two-way ANOVA. Beta-diversity was assessed by visualizing the differences in community composition between samples in a non-metric multidimensional scaling (NMDS) plot, using the R package phyloseq (McMurdie and Holmes, 2013). Distances between samples were derived from a Bray–Curtis dissimilarity matrix. To test for compositional differences between communities at Bloom stations and Low-Chl stations and in different depth intervals, a two-way permutation multivariate analysis of variance was conducted using the function adonis in the R package 'vegan' (Oksanen *et al*., 2020).

Differences in the abundance of ASVs at Bloom and Low-Chl stations were identified based on significant log2-fold changes, calculated using the R package DESeq2 (Love *et al*., 2014). The design formula included the sample types Bloom station and Low-Chl station as well as sampling depth as factors accounting for major sources of variation in the 16S rRNA gene sequence data. Likewise, diatom-dominated stations and stations with higher *Phaeocystis* proportions as well as sampling depth were used as factors to explore the significance of phytoplankton composition for the differential abundance of ASVs. In both cases, a local fit was chosen after inspecting the plot of dispersion estimates. Significance was accepted at $p_{adjusted} \leq 0.01$.

Co-occurrence network analysis

The co-occurrence network analysis included samples collected in the top 35 m of the water column and the ASVs present in at least 10% of these samples. The proportions of ASVs obtained from the sequence analysis of

the 16S rRNA gene were multiplied by bacterial cell numbers to estimate abundance. DCCHO and DAA concentrations (nmol L^{-1}) were also included. For the resulting subset of 237 ASVs, 10 sugars and 13 amino acids in 50 samples, a correlation matrix with pairwise Pearson correlation coefficients was generated using the R package Hmisc (Frank, 2021). False-positive results were excluded by adjusting the *p*-values using the multiple testing correction by the Benjamini–Hochberg method (Benjamini and Hochberg, 1995). Correlations between two ASVs and between ASVs and sugars and amino acids respectively, in which the *r* coefficient was ≥0.6 and the significance level was $p < 0.01$ were used to reconstruct the network. The network structure was explored and visualized using the R package igraph (Csardi and Nepusz, 2006). Network nodes represented ASVs, sugars and amino acids, and edges indicated strong and significant correlations between the nodes. Community detection was conducted using the fast greedy modularity optimization algorithm (Newman, 2004).

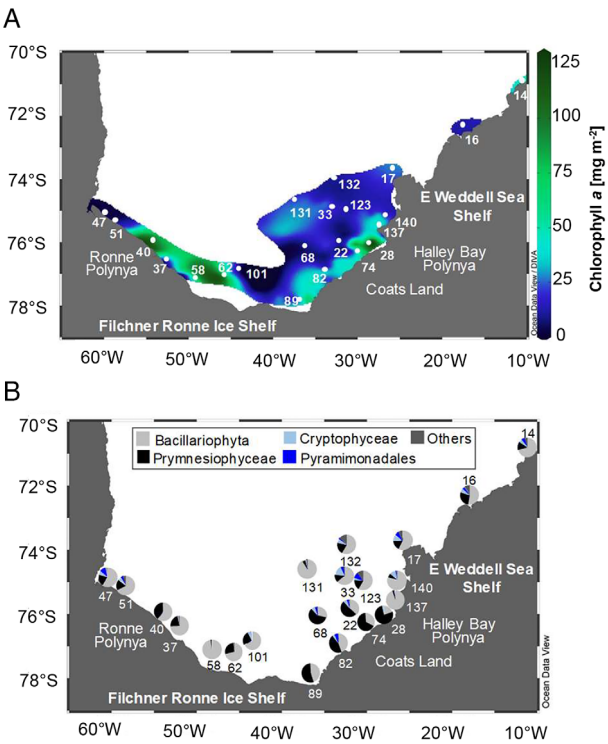

Fig. 1. Environmental conditions at sampling stations along the eastern Weddell Sea Shelf and the Filchner Ronne Ice Shelf.
A. Depth-integrated chlorophyll *a* concentrations. Three additional sampling stations located further north at Maud Rise (64.0–66.7°S) are not shown on the map.
B. Phytoplankton community composition as derived from plastidial sequences in the 16S rRNA gene libraries.

Results

Environmental context

Samples were collected at 22 stations along the eastern Weddell Sea shelf and the Filchner Ronne Ice Shelf and at three stations further north in the region of the submarine plateau Maud Rise (64.0–66.7°S) from the end of January to the end of February 2018 (Fig. 1A). Sampling along the shelf included the Halley Bay Polynya and the Ronne Polynya (Fig. S1). Sea surface temperatures of −1.8°C to −0.2°C were recorded along the shelves, and higher surface temperatures (1.8°C on average) at Maud Rise (64.0–66.7°S). Salinity along the shelves ranged from 33.1 to 34.4 at the surface and from 34.1 to 34.6 at 100 m depth. Surface salinity at the eastern Weddell Sea shelf was lower and more variable than at the Filchner Ronne Ice Shelf. The average surface concentrations of nitrate, phosphate and silicate were 23.3 ± 5.0, 1.7 ± 0.3 and 44.3 ± 9.4 µmol L^{-1} respectively.

Chl-*a* concentrations integrated over the top 100 m of the water column were highly variable along the shelves, ranging from 3.0 to 157.2 mg m^{-2} (Fig. 1A). Based on the depth-integrated Chl-*a* concentrations, shelf stations were grouped into nine Bloom stations (48.0–157.2 Chl-*a* mg m^{-2}, average 82.8 mg Chl-*a* m^{-2}) and 13 low-chlorophyll (Low-Chl) stations (3.0–31.0 mg Chl-*a* m^{-2}, average 12.3 mg Chl-*a* m^{-2}) to explore the effects of phytoplankton blooms on DOM, bacterioplankton activity and community composition (Fig. 1A, Table S1). At the Bloom stations, the highest Chl-*a* concentrations of 1.4–5.2 µg L^{-1} were measured in the upper 35 m of the water column. Seven of the nine Bloom stations were located in the Halley Bay Polyna (stations 28, 74, 137) and the Ronne Polynya (stations 37, 40, 58, 62) respectively, ice-free zones produced by katabatic winds (Fig. 1A). Two Bloom stations outside these polynyas were located east of the Halley Bay Polynya (station 14) and at the Filchner Ice Shelf (station 89). At five Bloom stations (stations 14, 28, 40, 58, 62, 74), NCP as a time-integrated measure of productivity could be estimated from the depletion of nitrate in the upper mixed layer. Bloom stations showed variable NCP, ranging from 1.1 to 6.9 mol C m^{-2} (average 4.2 mol C m^{-2}) (Table S1).

Sequences of chloroplasts in the 16S rRNA gene libraries provided insight into the phytoplankton composition (Decelle *et al*., 2015). Most stations were strongly dominated by diatom assemblages (Fig. 1B). The dominant diatom species was *Corethron pennatum*, which accounted, on average, for 15% of the chloroplast sequences, followed by *Fragilariopsis cylindrus*, *Proboscia alata*, and two unclassified species, with average contributions of 5%–9% each. At seven stations, including four Bloom stations, a large proportion (≥40%) of the chloroplast sequences were assigned to the prymnesiophyte *Phaeocystis* sp. (Fig. 1B).

Concentrations and composition of dissolved organic matter

The concentration of DOC at stations along the shelves was, on average, 54 ± 17 μmol L^{-1} at the surface and 47 ± 12 μmol L^{-1} at 100 m depth (Table 1). Integrating the concentrations over 100 m depth resulted in an average areal concentration of 4.81 ± 0.61 mol DOC m^{-2}. DOC concentrations at the Bloom stations did not significantly differ from those at the Low-Chl stations (Welch's *t*-test, $t = -0.17$, $df = 16.27$, $p = 0.87$). In contrast to bulk DOC, the concentrations of DAA and high-molecular-weight (>1 kDa) DCCHO at 0–35 m depth were significantly higher at Bloom stations than at Low-Chl stations [DAA: Two-way ANOVA, Depth: $F_{1,112} = 53.39$, $p < 0.001$; Sample Type (Bloom, Low-Chl): $F_{1,116} = 20.27$, $p < 0.001$; Depth × Sample Type: $F_{1,112} = 17.66$, $p < 0.001$; DCCHO: Two-way ANOVA, depth: $F_{1,112} = 38.35$, $p < 0.001$; sample type (Bloom, Low-Chl): $F_{1,116} = 15.41$, $p < 0.001$; depth × sample type: $F_{1,112} = 14.61$, $p < 0.001$] (Table 1). The average DAA and DCCHO contribution to bulk DOC of all samples collected at 0–35 m depth was 1.4 ± 0.5% and 3.2 ± 1.3% respectively. The average ratio of DCCHO: DAA increased from 2.3 at 0–35 m depth to 3.2 at 100 m depth, revealing a stronger depletion of amino acids than of carbohydrates with increasing depth (Table 1). Stations with elevated *Phaeocystis* contributions (≥40% of chloroplast sequences) had significantly higher DCCHO: DAA ratios than stations that were diatom-dominated [Two-way ANOVA, Depth: $F_{1,112} = 17.53$, $p < 0.001$; Sample Type (Bloom, Low-Chl): $F_{1,116} = 5.54$, $p < 0.05$; Depth × Sample Type: $F_{1,112} = 5.53$, $p < 0.05$].

The DAA composition was dominated by glycine that accounted on average for 38 and 43 mol% of DAA at 0–35 m and 100 m depth respectively. Aspartic acid, glutamic acid, alanine and serine contributed 8–14 mol% each to DAA (Table S2). A PCA of DAA composition at 0–35 m depth partially separated Bloom stations from Low-Chl stations on PC1, although with some overlap between the two sample types (Fig. 2A). A PERMANOVA confirmed small but statistically significant compositional differences between the DAA composition at Bloom stations and Low-Chl stations, while the phytoplankton composition had no significant effect [Sample Type (Bloom, Low-Chl): $R^2 = 0.09$, $F_{1,40} = 4.06$, $p = 0.02$; Phytoplankton (Diatoms, *Phaeocystis*): $R^2 = 0.03$, $F_{1,40} = 1.56$, $p = 0.17$; Sample Type × Phytoplankton: $R^2 = 0.02$, $F_{1,40} = 1.13$, $p = 0.30$]. The loadings of leucine, glutamic acid, phenylalanine, arginine, γ-aminobutyric acid and glycine on PC1 revealed their influence on compositional differences between Bloom stations and Low-Chl stations (Fig. 2A).

The dominant carbohydrates in DCCHO along the shelves were glucose and mannose/xylose, evidenced by average proportions of 34 and 35 mol% respectively, at 0–35 m depth. Galactose, fucose, rhamnose, arabinose and the amino sugar glucosamine contributed 1–11 mol% to DCCHO, in contrast to the amino sugar galactosamine and the acidic sugars glucuronic acid and galacturonic acid, each with contributions of ≤1 mol% (Table S3). PCA revealed that differences in the DCCHO composition between Bloom and Low-Chl stations were combined with a separation of strongly diatom-dominated stations from stations with higher shares of *Phaeocystis* sp. on PC2 (Fig. 2B). A PERMANOVA confirmed that both the bloom stage and the interaction of bloom stage and phytoplankton composition explained significant proportions of variation in the DCCHO composition [Bloom stage (Bloom, Low-Chl): $R^2 = 0.05$, $F_{1,40} = 2.94$, $p = 0.05$; Phytoplankton (Diatoms, *Phaeocystis*): $R^2 = 0.13$, $F_{1,40} = 7.74$, $p = 0.002$; Sample Type × Phytoplankton: $R^2 = 0.13$, $F_{1,40} = 7.81$, $p = 0.001$]. The loadings of carbohydrates on the first two principal components indicated enrichments of fucose, rhamnose, galactose, glucosamine and galactosamine at diatom-dominated Bloom-stations, and the enrichment of glucose in DCCHO of diatom-dominated Low-Chl stations. Stations with elevated *Phaeocystis* contributions had larger shares of arabinose and mannose/xylose (Fig. 2B).

Table 1. Concentration and composition of dissolved organic matter at Bloom stations and Low-Chl stations.

		DOC (μmol L^{-1})	DCCHO (nmol L^{-1})	DCCHO (% DOC)	DAA (nmol L^{-1})	DAA (% DOC)	DCCHO:DAA
0–35 m	All stations	54 ± 17	322 ± 139	3.2 ± 1.3	260 ± 152	1.4 ± 0.5	2.3 ± 0.9
	Bloom	53 ± 18	408 ± 172	3.8 ± 1.8	359 ± 186	1.7 ± 0.6	2.1 ± 1.1
	Low-chl	55 ± 18	263 ± 64	2.9 ± 0.9	191 ± 65	1.3 ± 0.4	2.5 ± 0.8
40–60 m	All stations	49 ± 12	240 ± 69	2.7 ± 0.9	153 ± 69	0.9 ± 0.3	3.1 ± 1.3
	Bloom	45 ± 5	258 ± 74	3.0 ± 0.9	175 ± 92	1.1 ± 0.4	3.0 ± 1.5
	Low-chl	52 ± 15	228 ± 64	2.4 ± 0.9	139 ± 47	0.8 ± 0.2	3.1 ± 1.2
75–100 m	All stations	47 ± 12	205 ± 49	2.6 ± 0.9	119 ± 35	0.8 ± 0.2	3.2 ± 0.8
	Bloom	48 ± 13	208 ± 49	2.6 ± 0.9	126 ± 50	0.8 ± 0.3	3.1 ± 0.9
	Low-chl	46 ± 12	202 ± 50	2.6 ± 0.9	115 ± 18	0.8 ± 0.2	3.2 ± 0.8

DOC: dissolved organic carbon, DCCHO: dissolved combined carbohydrates, DAA: dissolved amino acids.

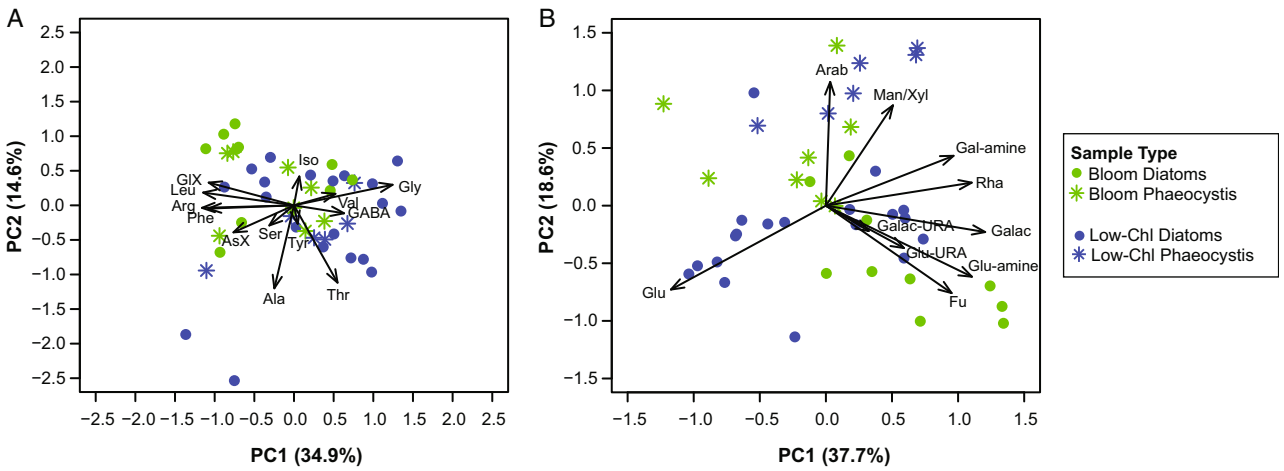

Fig. 2. Principal component analysis of (A) dissolved amino acid and (B) dissolved combined carbohydrate composition at 0–35 m depth. Bloom stations are shown in green and low-chlorophyll (Low-Chl) stations in blue. Strongly diatom-dominated stations and stations with larger contributions of *Phaeocystis* sp. are shown as different symbols.

Community composition of bacterioplankton

Illumina amplicon sequencing of the V3–V4 hypervariable region of both the 16S rRNA gene and the 16S rRNA yielded a final dataset of 7 590 245 sequences from 270 samples.

Sequences of the 16S rRNA gene comprised 1137 ASVs affiliated with *Bacteria* and 50 ASVs affiliated with *Archaea* (Fig. S3). Based on averages across all stations, the dominant bacterial classes *Bacteroidia*, *Alphaproteobacteria* and *Gammaproteobacteria* comprised 22%, 19% and 29% of the ASVs of the 16S rRNA gene respectively, and contributed 28 ± 14%, 42 ± 10% and 21 ± 8% respectively, to the sequences of the 16S rRNA gene (Fig. 3). Proportions of the 16S rRNA gene sequences revealed different vertical trends in the upper 100 m of the water column for the major classes of Weddell Sea bacterioplankton. *Bacteroidia* decreased over depth, from 38 ± 14% at 0–5 m to 16 ± 8% at 100 m. Likewise, the proportion of sequences assigned to *Bacteroidia* decreased from 21 ± 8% at 0–5 m to 7 ± 4% at 100 m (Fig. 3). *Alphaproteobacteria* in total showed only minor depth-related variation. In contrast, the sequence proportion affiliated with the *Roseobacter* clade decreased from 27 ± 11% at the surface to 4.9 ± 3.5% at 100 m respectively (Fig. 3). For *Gammaproteobacteria*, the proportion of 16S rRNA gene sequences increased from 14 ± 8% at 0–5 m to 24 ± 7% at 100 m depth. Similarly, the sequence proportion of *Archaea* increased from 0.2 ± 0.4% at the surface to 14 ± 8% at 100 m depth (Fig. 3). Archaeal ASVs were assigned to *Thermoplasmata* (25 ASVs), *Nitrososphaeria* (21 ASVs), *Nanoarchaeia* (three ASVs) and *Halobacteria* (one ASV) and strongly dominated by the candidate genus *Nitrosopumilus* (class *Nitrososphaeria*) and the Marine Group II (class *Thermoplasmata*), which at 100 m depth comprised 82 ± 8% and 17 ± 8% of archaeal sequences respectively (Fig. 3).

Sequences of the 16S rRNA revealed a similar taxonomic composition (Fig. S2). However, the comparison of 16S rRNA gene sequences and 16S rRNA sequences revealed an underrepresentation of the SAR11 Clade in the rRNA sequences and an overrepresentation of *Gammaproteobacteria* (Fig. 3 and Fig. S2).

The Chao1 index and the Shannon index revealed that richness and diversity of 16S rRNA gene sequences respectively were significantly higher at Low-Chl stations than at Bloom stations (Table S4). Values for both indices increased with sampling depth (Table S4). In all depth intervals, the Chao1 index of the 16S rRNA sequences showed higher values than the Chao1 index of 16S rRNA gene sequences (Table S4).

Changes in the taxonomic composition of the 16S rRNA gene sequences over depth as well as the differences between Bloom stations, Low-Chl stations and the northern stations at Maud Rise were resolved by a two-dimensional NMDS plot based on a Bray–Curtis dissimilarity matrix (Fig. 4A). The position of samples along the first axis reflected gradual changes in community composition over depth. Samples collected at 0–5 and 20–35 m were more dissimilar from each other than samples of other consecutive depth intervals. The second axis separated Bloom stations, Low-Chl stations and the three northern stations at Maud Rise. Sequences at the Maud Rise stations comprised 163 ASVs that were not prevalent at Bloom stations and Low-Chl stations. These unique ASVs comprised on average 2.3% of the sequences. A PERMANOVA of Bray–Curtis dissimilarities revealed that both bloom stage and sampling depth significantly affected the community composition along

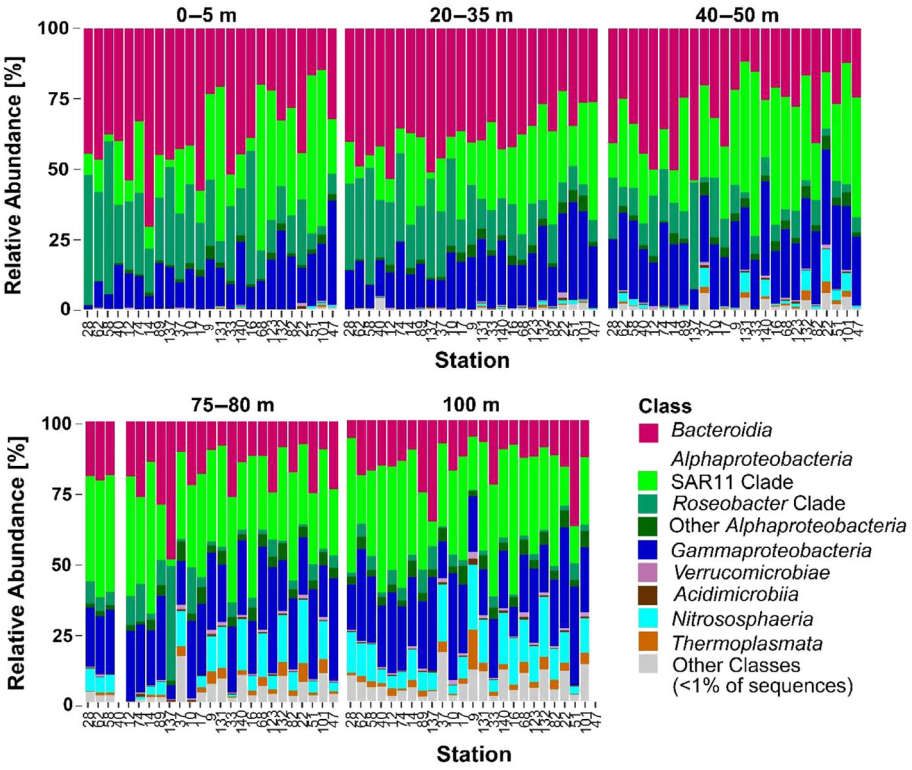

Fig. 3. Major classes in Weddell Sea bacterioplankton. Composition of the 16S rRNA gene sequences. Stations are ordered according to their chlorophyll *a* concentration, from highest (station 28) to lowest (station 47). Classes with median proportions ≥1% (across all samples) are shown individually. *Alphaproteobacteria* are further split into the *Roseobacter* clade, the SAR11 clade and other groups.

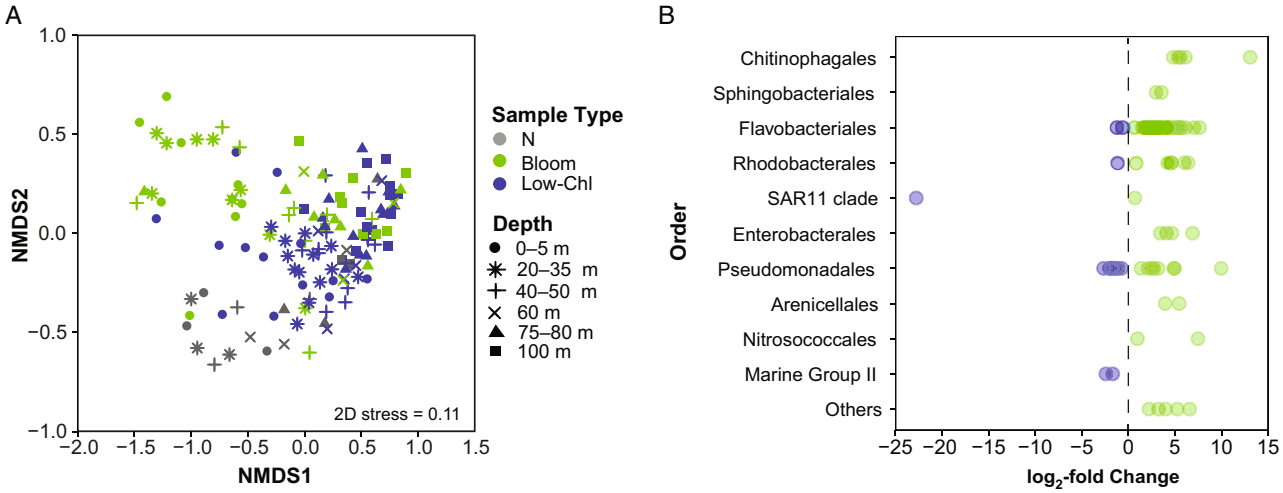

Fig. 4. Variation in bacterioplankton community composition.
A. NMDS plot. Bloom stations are shown in green, low-chlorophyll (Low-Chl) stations in blue and the northern stations (N) at 64.0–66.7°S in grey. Depth intervals are indicated by different symbols.
B. DESeq2 analysis of differentially abundant ASVs at Bloom stations and Low-Chl stations. ASVs with significantly larger proportions at Bloom stations (log2-fold change >0) are shown in green, and those with significantly higher proportions at Low-Chl stations in blue (log2-fold change <0).

the shelves, without a significant interaction of the two parameters [Depth: $R^2 = 0.22$, $F_{5,116} = 8.91$, $p = 0.001$; Sample Type (Bloom, Low-Chl): $R^2 = 0.15$, $F_{2,116} = 15.04$, $p = 0.001$; Depth × Sample Type: $R^2 = 0.06$, $F_{10,116} = 1.31$, $p = 0.09$].

Bloom stations and Low-Chl stations shared 67% of the ASVs. These shared ASVs comprised at least 94% of the sequences at the shelf stations. Differences between the sequence proportions at Bloom stations and Low-Chl stations were further explored in a DESeq2

analysis, which revealed 78 differentially abundant ASVs assigned to 11 orders (Fig. 4B and Fig. S3). Of these ASVs, 13 ASVs comprised ≥1% of the 16S rRNA gene sequences at 20–35 m, the depth of maximum Chl-*a* concentrations. Ten abundant ASVs assigned to the genera *Polaribacter*, *Ulvibacter* (both *Flavobacteriales*), *Yoonia-Loktanella*, *Sulfitobacter*, *Planktomarina* (all *Rhodobacterales*), the SAR92 clade (*Pseudomonadales*) and two unclassified genera of the families *Saprospiraceae* (*Chitinophagales*) and *Nitrincolaceae* (*Pseudomonadales*), respectively, were significantly enriched at Bloom stations. Three dominant ASVs affiliated with the NS4 Marine Group, the SAR86 Clade and the SUP05 Cluster showed significantly higher proportions at Low-Chl stations (Fig. 4B).

Spatial variation of prokaryotic key players along the shelves

The spatial variation of the dominant lineages in the upper mixed layer of the southern Weddell Sea was explored by compiling the abundances of the dominant taxa at 20–35 m, the depth of the Chl-*a* maximum (Fig. 5). The relative sequence proportions of the 20 most abundant ASVs ranged from 1.1% [SUP05 cluster (ASV3) and SAR86 clade (ASV25)] to 17.6% [SAR11 clade Ia (ASV1)]. Together, they accounted for 55%–78% of all sequences at 20–35 m depth. According to the results of the DESeq2 analysis, the 20 most abundant ASVs were classified as bloom-responsive taxa (log2-fold change >0), low-chlorophyll specialists (log2-fold change <0) and not differentially abundant (no significant change) (Figs 4B and 5). The bloom-responsive genus *Polaribacter* was represented by three abundant ASVs that differed in their spatial distributions along the shelves. *Polaribacter*-affiliated sequences at the Filchner-Ronne Ice Shelf were dominated by ASV8, while at the Eastern Weddell Sea Shelf ASV8 and ASV23 were detected in equal proportions. *Polaribacter*-affiliated ASV34 was more prevalent at the northern stations (64.0–66.7°S) than at the shelves (Fig. 5). *Yoonia-Loktanella* (ASV12) and *Sulfitobacter* (ASV14) showed pronounced maxima at stations located within the Halley Bay Polynya and the Ronne Polynya (Fig. 5). The bloom-responsive SAR92 clade (ASV17) and ASV44, an unclassified member of the family *Saprospiraceae*, were associated with *Phaeocystis* sp. (Fig. S4). Sequence proportions accounted on average for only 0.3% and 0.7% for ASV44 and the SAR92 clade respectively, at strongly diatom-dominated stations but for 3.9% and 3.5% at stations with larger shares of *Phaeocystis* sp.

Depth profiles of the bloom-responsive ASVs revealed that the abundances of *Polaribacter*, *Sulfitobacter* and *Yoonia-Loktanella* were highest at 0–5 m and steeply declined below the surface, while the SAR92 clade and ASV7, and unclassified member of the family

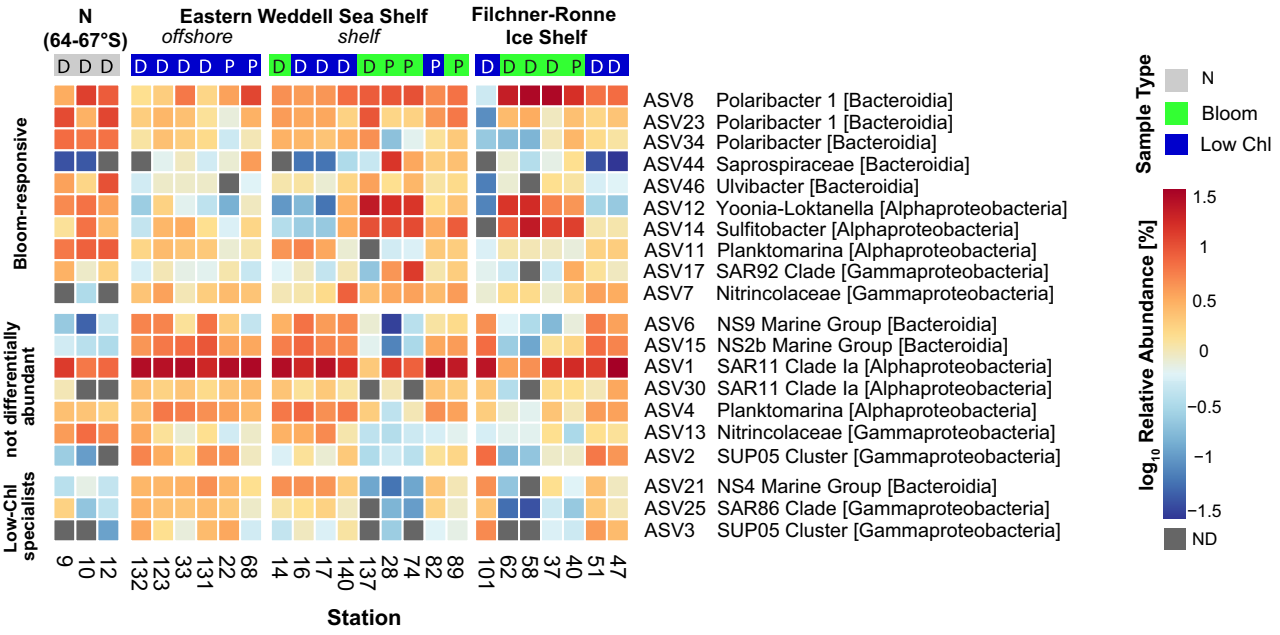

Fig. 5. Spatial distribution of the 20 dominant ASVs at 20–35 m depth. Panels of the heatmap show ASVs with larger proportions at Bloom stations (bloom-responsive, top), with equal proportions at Bloom and Low-Chl stations (not differentially abundant, middle), and with larger proportions at Low-Chl stations (low-Chl specialists, bottom), as derived from the DESeq2 analysis. Letters in the top colour bar indicate stations with strongly diatom-dominated phytoplankton (D) and stations with larger shares of *Phaeocystis* sp. (P).

Nitrincolaceae, showed highest abundance below the pycnocline at 40–50 m depth (Fig. S5). ASVs assigned to the NS4 marine group, the SAR86 clade and the SUP05 cluster were classified as specialists for Low-Chl stations by the DESeq2 analysis (Figs 4B and 5). Maxima of ASVs affiliated with the NS4 marine group (ASV21) and the SAR86 clade (ASV25) were often detected below the pycnocline at Low-Chl stations (Fig. S4).

In addition to the taxonomic classification, searches of the partial 16S rRNA gene sequences against the GenBank nucleic acid sequence database were performed to explore the similarity of the 20 dominant Weddell Sea ASVs with sequences in environmental samples (Table S5). Bloom-responsive *Yoonia-Loktanella* (ASV12), *Sulfitobacter* (ASV14), *Polaribacter* (ASV8, ASV23, ASV34), unclassified ASV44 (affiliated with *Saprospiraceae*) and unclassified ASV7 (affiliated with *Nitrincolaceae*) showed 100% sequence identity mostly with isolates and sequences obtained from Antarctic and Arctic marine systems (Table S5). Environmental sequences 100% identical to *Yoonia-Loktanella* (ASV12), *Sulfitobacter* (ASV14) and *Polaribacter* (ASV8) included sequences derived from sea ice. ASV7 (unclassified *Nitrincolaceae*) was 100% identical to the uncultivated Antarctic γ-Proteobacterium Ant4D3.

By contrast, sequences of the bloom-responsive *Ulvibacter* and the SAR92 clade as well as the dominant ASVs at Low-Chl stations, i.e. ASV21 (NS4 marine group), ASV25 (SAR86 clade) and ASV3 (SUP05 cluster), were 100% identical to sequences from both polar and temperate oceans (Table S5). The two dominant ASVs affiliated with the SUP05 cluster (ASV2 and ASV3) showed 100% identity with the sequences of the summer and winter communities in coastal surface waters of the Antarctic Peninsula (Grzymski *et al*., 2012) and were uniformly distributed over depth at the Weddell Sea shelves (Fig. S5).

Bacterial activity

Bacterial biomass production ranged from 2.5 to 53.8 mg C m^{-2} d^{-1} and was directly related to Chl-*a* concentrations across all stations in the Weddell Sea (linear regression, $r^2 = 0.55$, $p < 0.0001$, $n = 25$) (Fig. 6A). Depth-integrated bacterial production at Bloom stations was, on average, 2.7 times higher than at Low-Chl stations. Highest bacterial production of 0.84 ± 0.43 μg C L^{-1} d^{-1} was measured at Bloom stations at 0–40 m depth. Maximum growth rates of 0.44 and 0.53 d^{-1} were determined at Bloom stations at 20–35 m depth. The largest differences between Bloom stations and Low-Chl stations occurred at 40–75 m, where bacterial production and bacterial growth rates at Bloom stations were, on average, 3.4 times and 4.2 times higher than at Low-Chl stations respectively. Bacterial growth rates at Bloom stations exceeded those at Low-Chl stations in the upper mixed layer but also below the pycnocline [two-way ANOVA, Depth: $F_{1,112} = 38.97$, $p < 0.001$; Sample Type (Bloom, Low-Chl): $F_{1,116} = 59.06$, $p < 0.001$; Depth × Sample Type: $F_{1,112} = 0.44$, $p > 0.05$]. Cell numbers of both bacteria and nanoflagellates declined from the surface to 100 m depth without clear differences between Bloom stations and Low-Chl stations (Fig. S6). Differences in phytoplankton composition as inferred from chloroplast sequences in the 16S rRNA gene libraries had no consistent effect on bacterial activity and cell numbers of bacteria and nanoflagellates (Fig. 6B and Fig. S6).

Co-occurrence network of surface communities

A co-occurrence network analysis of surface communities was conducted to explore positive associations between different ASVs and between ASVs and DOM components (Fig. 7). The co-occurrence network consisted of 239 nodes and 1886 edges. It had a diameter of

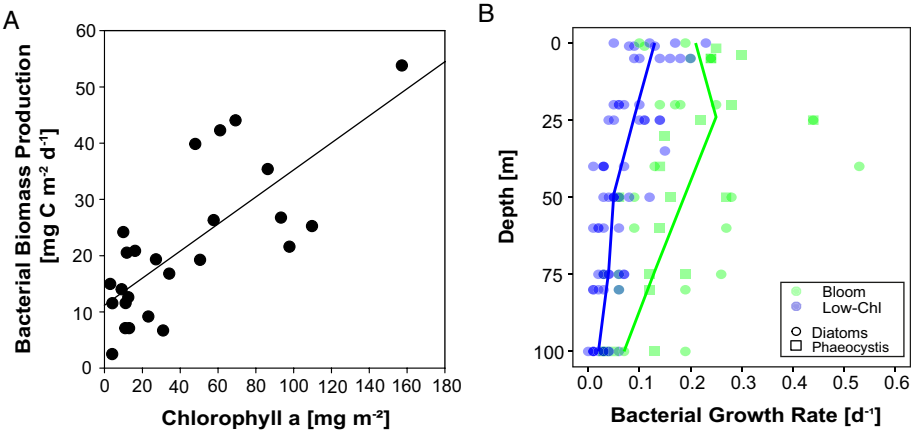

Fig. 6. Bacterial biomass production and growth.
A. Chlorophyll *a* concentrations (mg Chl-*a* m^{-2}) related to bacterial biomass production (mg C m^{-2} d^{-1}). Regression line: $y = 0.24x + 11.18$, $r^2 = 0.55$, $p < 0.0001$.
B. Depth profiles of growth rates (d^{-1}).

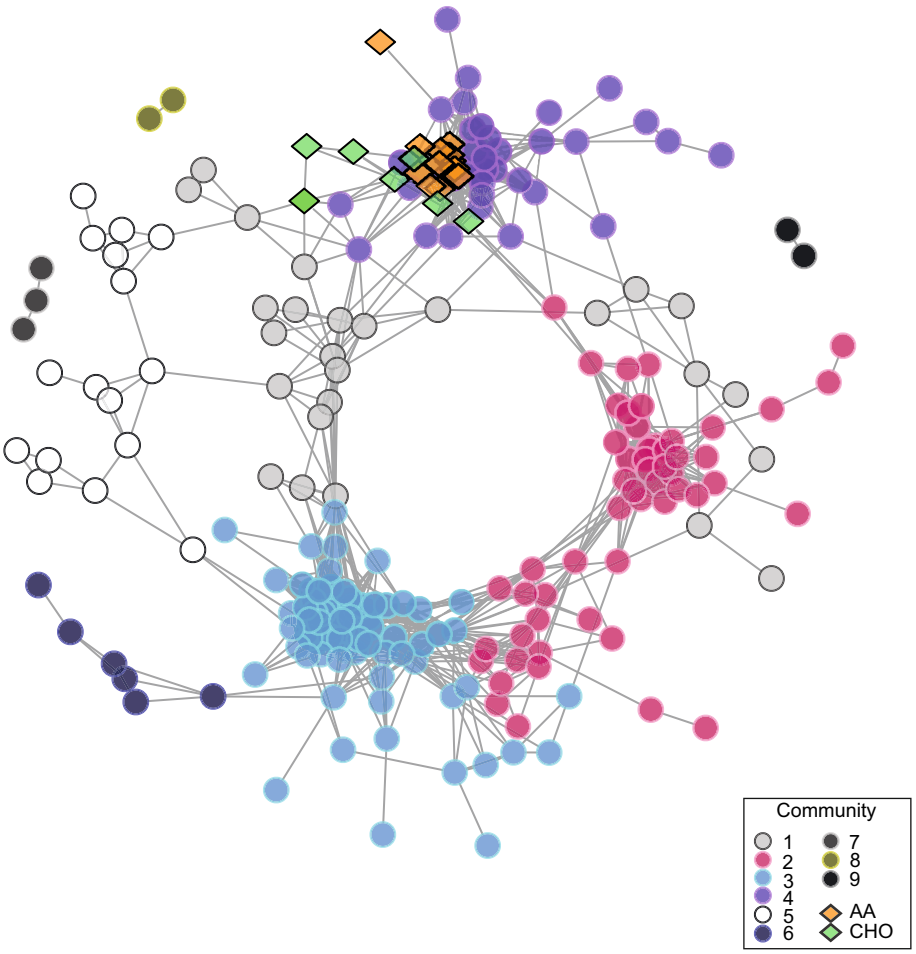

Fig. 7. Co-occurrence network of positive interactions between *Bacteria*, *Archaea*, amino acids and carbohydrates at 0–35 m depth. Connections indicate significant positive correlations (Pearson's $r > 0.6$, $p < 0.01$). Nodes represent ASVs (circles), amino acids (AA, orange diamonds) and carbohydrates (CHO, green diamonds). ASVs are colour-coded by community.

8.2, a transitivity of 0.70 and an average path length of 4.3. A modularity of 0.59 based on greedy optimization yielded a modular structure that included nine communities (Fig. 7; Table 2). Three of those communities (communities 7–9) consisted of only two to three vertices and were disconnected from the other six interconnected communities (1–6), each of which consisted of 6–75 vertices (Fig. 7; Table 2).

All analysed amino acids and five of the 10 analysed sugars were part of community 4 (Fig. 7). In that community, 33% of the edges were linkages between ASVs and either amino acids or sugars. Community 4 included 42% of the ASVs identified in the DESeq2 analysis as bloom-responsive taxa, including the abundant ASV8 (*Polaribacter 1*), ASV12 (*Yoonia-Loktanella*) and ASV14 (*Sulfitobacter*). Linkages to at least one sugar or amino acid were determined for 66% of the nodes in community 4.

Community 3 had the highest average degree, with at least twice as many edges between ASVs than detected in the other communities (Table 2). Thirteen of the 14 ASVs present in the co-occurrence network and enriched at Low-Chl stations according to the DESeq2 analysis were members of community 3, including the abundant ASV21 (NS4 Marine Group) and ASV3 (SUP05 Cluster).

Discussion

Organic matter availability and its relevance for heterotrophic bacterial activity

The Halley Bay Polynya and the Ronne Polynya were identified in this study as hotspots of phytoplankton standing stocks and microbial carbon cycling in the Weddell Sea. Maxima in Chl-*a*, NCP, dissolved proteins and carbohydrates along the shelves were determined in the two polynyas, evidence of their importance for biological productivity throughout the summer season. In line with previous observations from the Weddell Sea and the Ross Sea (von Bröckel, 1985; Arrigo *et al*., 2000), strongly diatom-dominated blooms occurred in the shallow surface mixed layers of the Ronne Polynya, whereas blooms with larger proportions of *Phaeocystis* sp. developed in more deeply mixed waters of the eastern Weddell Sea Shelf. Despite the development of

Table 2. Topological features of the co-occurrence network.

	Nodes				Edges	Average degree	Average path length	Transitivity
	Total	Bacteroidia (%)	Alphaproteobacteria (%)	Gammaproteobacteria (%)				
Whole Network	239	34	19	37	1886	15.8	4.3	0.70
Community 1	27	62	4	27	55	4.1	3.3	0.53
Community 2	54	41	19	35	301	11.1	2.6	0.68
Community 3	75	20	31	33	947	25.3	1.9	0.73
Community 4	54	34	11	51	456	9.2[a] (16.9[b])	2.1	0.70
Community 5	16	44	6	31	25	3.1	3.0	0.52
Community 6	6	67	0	33	9	3.0	1.5	0.71

[a]Average degree between ASVs.
[b]Average degree including edges between ASVs and CHO/AA.

phytoplankton blooms along the shelf, DOM accumulation was low compared to temperate marine systems. Average DOC concentrations at the surface and at 20–35 m depth exceeded the concentrations at 100 m depth by 3–14 μmol L^{-1}. This range is similar to that reported in other studies of spring blooms in the Southern Ocean but substantially lower than the range in temperate marine systems such as the North Sea (ΔDOC 30–50 μmol L^{-1}) and the Mediterranean Sea (ΔDOC ∼30 μmol L^{-1}) (Kähler *et al*., 1997; Wiebinga and De Baar, 1998; Ogawa *et al*., 1999; Trabelsi and Rassoulzadegan, 2011; Sperling *et al*., 2017). Low DOC production along the Weddell Sea shelves might be explained by the low partitioning of primary production into DOM. During the spring bloom in the Ross Sea, only 10% of organic carbon is allocated to the dissolved pool (Carlson *et al*., 2000) compared to 86% of the bloom-produced carbon in the oligotrophic Sargasso Sea (Carlson *et al*., 1998). In addition, the results of experimental studies suggest that nutrient-replete conditions like in the southern Weddell Sea reduce the release of DOC by phytoplankton exudation (Engel *et al*., 2013).

Despite the limited buildup of DOC stocks, bacterial production and growth along the shelves responded strongly to the development of phytoplankton blooms. The direct relationship between the Chl-*a* concentration and bacterial biomass production as well as the significantly higher bacterial growth rates at Bloom stations than at Low-Chl stations strongly suggested that the low availability of fresh phytoplankton-derived organic matter constrained bacterial growth. Heterotrophic bacterial growth rates of 0.10–0.53 d^{-1} (average 0.25 d^{-1}) in the upper mixed layer of Bloom stations were similar to values reported for the Equatorial Pacific Ocean (0.11–0.16 d^{-1}) and the North Atlantic Ocean (0.1–0.3 d^{-1}), where the seawater temperature is 10°C–20°C higher (Ducklow *et al*., 1993; Kirchman *et al*., 1995, 2009a).

At the Bloom stations, bacterial growth rates were also elevated below the pycnocline, although in these deeper waters the concentrations of DOC, DHAA and DCCHO were similar to those at Low-Chl stations. This observation indicates that sinking phytoplankton-derived particles sustained a significant share of bacterial biomass production. High bacterial activity at mid-water depth was also reported for the Ross Sea and the Amundsen Sea Polynyas, where high bacterial production coincided with a strong reduction in particle fluxes in this depth interval (Williams *et al*., 2016). In addition, the tighter coupling of bacterial production with Chl-*a* than with primary production in coastal waters of the Antarctic Peninsula suggests that heterotrophic bacterioplankton in Antarctic marginal seas relies on DOC production at various trophic levels and not primarily on the direct release of DOC by phytoplankton (Kim and Ducklow, 2016).

Overall, our results revealed a strong coupling of bacterial growth to phytoplankton along the Weddell Sea shelves and a high potential for bacterial carbon remineralization in the upper 100 m of the water column.

Molecular composition and transformation of DOM

In line with the low DOC concentrations, the concentrations of DAA and DCCHO in the Weddell Sea were also substantially lower than in temperate oceans. A comparison of the concentrations in the Weddell Sea with those in tropical oceans and in the Arctic Ocean showed a stronger depletion of DCCHO than of DAA. The average surface DCCHO concentration in the Weddell Sea (322 nmol L^{-1}) was almost four times lower than in the eastern tropical South Pacific, 2.5-fold lower than in Fram Strait (Arctic Ocean), and ∼80 nmol L^{-1} lower than the concentrations determined in the central Arctic Ocean (Loginova *et al*., 2019; von Jackowski *et al*., 2020; Piontek *et al*., 2021). At the same time, the average surface DAA concentration of 259 nmol L^{-1} determined in the Weddell Sea was only about twofold lower than in the eastern tropical South Pacific, similar to the concentrations in Fram Strait and 60–90 nmol L^{-1} higher than the

concentrations in the central Arctic Ocean and East Siberian shelf seas (Loginova *et al*., 2019; von Jackowski *et al*., 2020; Piontek *et al*., 2021). A study investigating the optical properties of DOM in the Amundsen Sea also reported the relative enrichment of proteins in DOM, indicated by a high tyrosine-like fluorescence (Chen *et al*., 2019). Our field data cannot resolve the mechanisms sustaining carbohydrate depletion and protein enrichment in Weddell Sea DOM. The nutrient-replete conditions along the shelves may have reduced the production of phytoplankton-derived carbohydrates. It has been experimentally demonstrated that the accumulation of dissolved carbohydrates and carbohydrate-rich gels is lower during nutrient-replete phytoplankton growth than under nutrient limitation (Engel *et al*., 2002; Granum *et al*., 2002; Borchard and Engel, 2012). A biological process that may support DAA enrichment is the intense allocation of photosynthetic carbon into phytoplankton proteins, as reported for communities in the Amundsen Sea Polynya (Song *et al*., 2016). Furthermore, copepods feeding on phytoplankton cells can incidentally enhance the release of amino acids into the dissolved pool (Riemann *et al*., 1986).

A prominent feature of the DAA of the Weddell Sea was the consistently large share of glycine (41 $\pm$ 6%), which was 11%–20% larger than the share in the Sargasso Sea, the North Pacific subtropical gyre and the eastern tropical South Pacific (Kaiser and Benner, 2009; Loginova *et al*., 2019), but similar to the share in the waters north of the Antarctic Peninsula at 59–63°S (~35%) (Shen *et al*., 2017). A high glycine content has been interpreted as an indicator of degraded and recalcitrant DOM (Nguyen and Harvey, 1997; Kaiser and Benner, 2009). However, a consistently large amount of glycine in the surface waters at Bloom stations suggests that also fresh DOM in the Weddell Sea was glycine-enriched. It was previously shown that the biomass of plankton at and south of the Antarctic Polar Front was enriched in glycine compared to the biomass of plankton north of the front (Ingalls *et al*., 2003). Hence, the solubilization of glycine-rich organic particles by bacterial extracellular enzymes may have led to glycine accumulation in DOM.

The molecular composition of carbohydrates was strongly influenced by phytoplankton-specific variations. At stations with larger shares of *Phaeocystis* sp., DCCHO were enriched in arabinose and mannose/xylose. Arabinose, mannose and xylose are major non-glucose carbohydrates in *Phaeocystis globosa* and *Phaeocystis pouchetii* (Biersmith and Benner, 1998; Alderkamp *et al*., 2007a). Bioassays further showed that the mucopolysaccharide fraction of *Phaeocystis globosa* is not susceptible to the abundant laminarin-degrading hydrolases of natural marine bacterioplankton (Alderkamp *et al*., 2007b). Our results provide further evidence that arabinose-, xylose- and mannose-containing polysaccharides are recalcitrant components in DOM. In the PCA, samples from both Bloom and Low-Chl stations with elevated *Phaeocystis* contributions were enriched in arabinose and mannose/xylose, suggesting that these polysaccharides were not degraded over short time-scales during and/or after bloom events. Polysaccharide-utilization loci encoding enzymes for the degradation of arabinose-, xylose- and mannose-containing polysaccharides have been found in *Flavobacteriia*, indicating that these carbohydrates can be accessed by at least some important lineages of marine bacterioplankton (Kappelmann *et al*., 2019).

Spatial variation in the diversity, structure and taxonomic composition of bacterial communities

To the best of our knowledge, this is the first taxonomic survey of Weddell Sea bacterioplankton using high-throughput sequencing on the Illumina platform. The taxonomic composition inferred from 16S rRNA gene sequences and 16S rRNA sequences was largely similar. Differences were mainly driven by taxa with small cell sizes such as the SAR11 clade and the *Candidatus Nitrosopumilus*-dominated *Thermoplasmata*. Previous studies suggested that the 16S rRNA sequences of environmental samples are at least enriched with ribosomes of active community members (Campbell *et al*., 2011; Denef *et al*., 2016). Given this assumption, the compositional similarity of 16S rRNA gene sequences and 16S rRNA sequences in our study suggests that the largest share of taxa in the Weddell Sea was putatively active. This is consistent with the conclusion by Salazar *et al*. (2019) that changes in the functioning of polar marine communities are primarily driven by community turnover rather than by changes in gene expression.

The dominant taxa in the Weddell Sea, i.e. *Polaribacter*, *Sulfitobacter*, *Yoonia-Loktanella*, *Ulvibacter*, the SAR11, SAR86, and SAR92 clades, and the NS2b, NS4 and NS9 marine groups, were also shown to be abundant in summer communities of the west coast of the Antarctic Peninsula, in the Amundsen Sea Polynya, Terra Nova Bay (Ross Sea), and at the central Kerguelen Plateau in the Indian sector of the Southern Ocean (Grzymski *et al*., 2012; Delmont *et al*., 2014; Luria *et al*., 2016; Liu *et al*., 2020). Hence, these lineages are likely part of a summer core community in Antarctic marginal seas. *Polaribacter* and the NS9 marine group (both *Flavobacteriales*) were further identified as important taxa in the latitudinal differentiation of bacterial communities from temperate to polar oceans (Salazar *et al*., 2019). Dominant ASVs were assigned to *Bacteroidia*, *Alphaproteobacteria* and *Gammaproteobacteria*, demonstrating that the genetic potential for sufficient adaptation to sub-zero

seawater temperature is phylogenetically widespread. Previous studies showed that cold ecosystems contain many microorganisms capable of only moderate cold adaptation (Bowman, 2017). A potential reason is that fast growth rates are not generally selected for in ecosystems with limited and ephemeral resources (Roller and Schmidt, 2015). Consequently, in very cold environments a perfect adaptation of growth to prevailing temperatures would not necessarily be advantageous (Bowman *et al*., 1997; Steven *et al*., 2008; Tuorto *et al*., 2014). The dominance of ubiquitous marine genera along the Weddell Sea shelves may point to moderate cold adaptation. An alternative explanation, however, is that these ubiquitous taxa achieve genetic variation enabling cold adaptation mostly at the species and/or ecotype level. Consistent with the assumption of species and/or ecotypes adapted to the polar marine environment, dominant sequences of the Weddell Sea affiliated with *Planktomarina*, *Sulfitobacter*, *Yoonia-Loktanella*, the SAR92 clade and the SAR86 clade showed 100% identity only with sequences from the cold ocean.

The strong response of bacterial biomass production to phytoplankton blooms along the Weddell Sea shelves was accompanied by distinct spatial changes in the taxonomic composition of surface bacterioplankton. Differences in the community composition between Bloom and Low-Chl stations were driven mainly by members of the orders *Flavobacteriales*, *Rhodobacterales*, *Cellvibrionales*, *Chitinophagales* and *Pseudomonadales*. Sequences affiliated with the bloom-responsive genera *Yoonia-Loktanella*, *Sulfitobacter* and *Polaribacter* showed 100% identity with sequences retrieved from sea ice samples, suggesting that representatives of these genera in the Weddell Sea can also cope with entrainment into highly saline brine channels. The flexibility to colonize both sea ice and surface seawater may contribute to the successful ecological strategy of these genera along the ice shelves. Their predominance in surface ocean communities during summer was potentially supported by the ability to utilize light as an energy source. Cultured representatives of *Polaribacter* were shown to contain the proteorhodopsin gene as well as genes encoding proteins conferring the ability to sense and respond to light (González *et al*., 2008). Sequences encoding the photosynthetic reaction centre PufL and PufM were identified in the genomes of *Yoonia-Loktanella* and *Sulfitobacter* (Imhoff *et al*., 2018). In contrast to other bloom-responsive lineages, the sequence proportions of *Loktanella*, *Sulfitobacter* and *Polaribacter* strongly declined from the surface to 40–50 m depth. Phototrophic energy production may explain this preference for the sea surface rather than for the depth of maximum Chl-*a* concentration (20–35 m).

Another successful metabolic strategy of bloom-responsive taxa was potentially the efficient utilization of specific DOM components. Cultivars of both *Yoonia-Loktanella* and *Sulfitobacter* possess genes encoding enzymes for the demethylation of dimethylsulfoniopropionate (DMSP), an organic osmolyte produced by many phytoplankton species (Bullock *et al*., 2017). Furthermore, the SAR92 clade and an unclassified member of the family *Saprospiraceae* (*Chitinophagales*) (ASV44) showed a clear preference for stations with elevated proportions of *Phaeocystis* sp. The prevalence of *Phaeocystis* sp. had a strong effect on the carbohydrate composition in the Weddell Sea. The substrate spectrum produced by *Phaeocystis sp*., which also includes DMSP and nitrogen-rich components, may shape the structure and composition of the associated bacterial communities (Delmont *et al*., 2014, 2015).

Heterotrophic lineages also dominated stations with low Chl-*a* concentrations. Hence, representatives of groups like the NS4 marine group and the SAR86 clade may be considered as specialists in coping with low organic matter availability at sub-zero temperatures. This observation is consistent with the description of seasonal niches of the NS4 marine group and the SAR86 clade before and/or after major phytoplankton bloom events in temperate marine systems (Treusch *et al*., 2009; Alonso-Sáez *et al*., 2015). The dominance of heterotrophic bacterial taxa at Low-Chl stations is in marked contrast to the winter surface communities, which have been shown to comprise up to 20% of chemolithoautotrophic archaea and bacteria (Massana *et al*., 1998; Murray *et al*., 1999; Grzymski *et al*., 2012). During summer, heterotrophs outcompeted chemolithoautotrophic assemblages in the Weddell Sea even below the ice, suggesting that already low concentrations of fresh organic matter were sufficient to induce a community shift. The dominance of heterotrophic communities at low organic matter concentration at the Weddell Sea shelves is consistent with the results of a seasonal study off the Antarctic Peninsula, where already ephemeral phytoplankton production at increasing daylight in late October resulted in increasing proportions of *Flavobacteriales* and decreasing proportions of chemolithoautotrophs (Luria *et al*., 2016). *Candidatus Nitrosopumilus*, the dominant archaeon in Antarctic surface communities during winter, showed elevated abundance at depths ≥75 m in our study. An experimental study revealed that *Nitrosopumilus maritimus* exhibited photosensitive growth and its growth rates significantly decreased already at low light intensities (15 $\mu E\ m^{-2}\ s^{-1}$) (Merbt *et al*., 2012). Therefore, light penetration at low ice concentrations and in ice-free waters may also have contributed to the low prevalence of

Candidatus Nitrosopumilus in Weddell Sea surface communities during summer. A feature shared by Antarctic winter and summer communities of the Weddell Sea was the prevalence of the SUP05 cluster (Grzymski *et al*., 2012). Recent studies recognized this cluster as a metabolically diverse lineage comprising autotrophic and heterotrophic members (van Vliet *et al*., 2021). Heterotrophic members have been commonly found in free-living bacterioplankton of the oxic ocean, suggesting that representatives of the SUP05 cluster in the surface Weddell Sea are consumers of organic carbon. However, it cannot be excluded that partial or incomplete sulfur oxidation and carbon fixation pathways allow thioautotrophic growth (Morris and Spietz, 2022). Furthermore, proteorhodopsin sequences affiliated with the SUP05 cluster were detected in the surface ocean (Olson *et al*., 2018). These findings suggest that, in Antarctic marine systems, the versatile metabolism of the SUP05 cluster provides it with a successful year-round strategy that may lead to competitive advantages over strictly heterotrophic and chemolithoautotrophic groups.

The differences in bacterial community composition between Bloom stations and Low-Chl stations were also reflected in the co-occurrence network. Bloom-responsive ASVs and specialists for low organic matter availability were largely included in different communities of the network. The average number of positive associations between ASVs in the community of low-organic matter specialists was at least twice as high as in other communities of the network, suggesting a larger number of positive interactions between low-organic matter specialists than between bloom-responsive ASVs. The high level of interaction at low availability of fresh organic matter is in agreement with observations from the temperate ocean, where the NS2b marine group, the NS4 marine group, and the SAR86 clade, i.e. abundant taxa in the Weddell Sea, were shown to participate in episodic events of synchronized growth (Alonso-Sáez *et al*., 2015). Interspecies interactions are increasingly recognized as a major biotic factor shaping plankton communities (Lima-Mendez *et al*., 2015). In particular, cross-feeding between species with streamlined genomes was shown to result in highly interconnected stable bacterial communities (Johnson *et al*., 2020). It can thus be assumed that beneficial interactions support the heterotrophic growth of communities in areas of low organic matter availability in the Weddell Sea.

Conclusion

Our results demonstrate the presence of highly active bacterioplankton along the ice shelves of the southern and eastern Weddell Sea. The spatial variation in heterotrophic bacterial activity and in taxonomic community composition was shown to be driven by the development of phytoplankton blooms in ice-free coastal polynyas. The extent of Antarctic sea ice has changed dramatically in the last ~50 years, from relatively gradual increases in the late 1970s to rapid decreases since 2014. Similar to other Antarctic marginal seas, the ice extent in the Weddell Sea decreased markedly during 2015–2018, when the record minimum was nearly reached (Parkinson, 2019; Turner *et al*., 2020). Our results show that phytoplankton and bacteria were tightly coupled during this phase of rapid ice loss, such that bacterial carbon re-mineralization increased in response to the increased availability of fresh organic matter in the expanding ice-free regions. In our study area, the two major coastal polynyas were shown to be hotspots of bacterial carbon recycling. The dominance of taxa like *Polaribacter*, *Sulfitobacter*, *Yoonia-Loktanella*, *Planktomarina*, the SUP05 cluster, and the SAR11 and SAR86 clades, in the southern Weddell Sea evidenced sufficient genetic adaption to the Antarctic marine environment by ubiquitous and phylogenetically diverse marine lineages.

Acknowledgements

We would like to thank the captain and the crew of RV *Polarstern* and the shipboard science party of the expedition PS111 for their great support during the cruise. Sandra Golde, Jon Roa and Christian Burmeister are greatly acknowledged for chemical measurements. Thanks to Katja Käding and Claudia Runkel for microbial cell counts. The authors also thank Johannes Werner for support in sequence analysis and Silke Lischka and Jan Michels for logistic support. This work was funded by the German Research Foundation (DFG) in the priority programme SPP 1158 'Antarctic Research with comparative investigations in Arctic ice areas' by grant PI 784/3-1 to Judith Piontek. Open Access funding enabled and organized by Projekt DEAL.

Data Availability

The primer-trimmed paired-end reads were deposited in the European Nucleotide Archive (Silvester *et al*., 2018) under project accession number PRJEB49387. Biogeochemical data and data on bacterial biomass production were archived in the Pangea data repository (https://doi.org/10.1594/PANGAEA.938700, https://doi.org/10.1594/PANGAEA.938702). The data were archived using the brokerage service of the German Federation for Biological Data (Diepenbroek *et al*., 2014).

References

Alderkamp, A.-C., Buma, A.G.J., and van Rijssel, M. (2007a) The carbohydrates of *Phaeocystis* and their degradation in the microbial food web. *Biogeochemistry* **83**: 99–118.

Alderkamp, A.C., Van Rijssel, M., and Bolhuis, H. (2007b) Characterization of marine bacteria and the activity of their enzyme systems involved in degradation of the algal storage glucan laminarin. *FEMS Microbiol Ecol* **59**: 108–117.

Alonso-Sáez, L., Díaz-Pérez, L., and Morán, X.A.G. (2015) The hidden seasonality of the rare biosphere in coastal marine bacterioplankton. *Environ Microbiol* **17**: 3766–3780.

Arrigo, K.R., DiTullio, G.R., Dunbar, R.B., Robinson, D.H., Van Woert, M., Worthen, D.L., and Lizotte, M.P. (2000) Phytoplankton taxonomic variability in nutrient utilization and primary production in the Ross Sea. *J Geophys Res Ocean* **105**: 8827–8846.

Arrigo, K.R., and van Dijken, G.L. (2003) Phytoplankton dynamics within 37 Antarctic coastal polynya systems. *J Geophys Res C Ocean* **108**: 21–27.

Benjamini, Y., and Hochberg, Y. (1995) Controlling the false discovery rate: a practical and powerful approach to multiple testing. *J R Stat Soc Ser B* **57**: 289–300.

Biersmith, A., and Benner, R. (1998) Carbohydrates in phytoplankton and freshly produced dissolved organic matter. *Mar Chem* **63**: 131–144.

Borchard, C., and Engel, A. (2012) Organic matter exudation by *Emiliania huxleyi* under simulated future ocean conditions. *Biogeosciences* **9**: 3405–3423.

Bowman, J.P. (2017) Genomics of psychrophilic bacteria and archaea. In *Psychrophiles: From Biodiversity to Biotechnology*, 2nd ed, Margesin, R. (ed). Berlin, Heidelberg: Springer, pp. 1–685.

Bowman, J.P., McCammon, S.A., Brown, M.V., Nichols, D. S., and McMeekin, T.A. (1997) Diversity and association of psychrophilic bacteri in Antarctic sea ice. *Appl Environ Microbiol* **63**: 3068–3078.

Bullock, H.A., Luo, H., and Whitman, W.B. (2017) Evolution of dimethylsulfoniopropionate metabolism in marine phytoplankton and bacteria. *Front Microbiol* **8**: 1–17.

Callahan, B.J., McMurdie, P.J., and Holmes, S.P. (2017) Exact sequence variants should replace operational taxonomic units in marker-gene data analysis. *ISME J* **11**: 2639–2643.

Callahan, B.J., McMurdie, P.J., Rosen, M.J., Han, A.W., Johnson, A.J.A., and Holmes, S.P. (2016) DADA2: high-resolution sample inference from Illumina amplicon data. *Nat Methods* **13**: 581–583.

Campbell, B.J., Yu, L., Heidelberg, J.F., and Kirchman, D.L. (2011) Activity of abundant and rare bacteria in a coastal ocean. *Proc Natl Acad Sci U S A* **108**: 12776–12781.

Carlson, C.A., Ducklow, H.W., Hansell, D.A., and Smith, W. O. (1998) Organic carbon partitioning during spring phytoplankton blooms in the Ross Sea polynya and the Sargasso Sea. *Limnol Oceanogr* **43**: 375–386.

Carlson, C.A., Hansell, D.A., Peltzer, E.T., and Smith, J. (2000) Stocks and dynamics of dissolved and particulate organic matter in the Southern Ross Sea, Antarctica. *Deep Res Part II Top Stud Oceanogr* **47**: 3201–3225.

Chen, M., Jung, J., Lee, Y.K., Kim, T.W., and Hur, J. (2019) Production of tyrosine-like fluorescence and labile chromophoric dissolved organic matter (DOM) and low surface accumulation of low molecular weight-dominated DOM in a productive Antarctic Sea. *Mar Chem* **213**: 40–48.

Csardi, G., and Nepusz, T. (2006) The igraph software package for complex network research. *InterJournal, Complex Systems 1695*. https://igraph.org

Decelle, J., Romac, S., Stern, R.F., Bendif, E.M., Zingone, A., Audic, S., *et al*. (2015) PhytoREF: a reference database of the plastidial 16S rRNA gene of photosynthetic eukaryotes with curated taxonomy. *Mol Ecol Resour* **15**: 1435–1445.

Delmont, T.O., Hammar, K.M., Ducklow, H.W., Yager, P.L., and Post, A.F. (2014) Phaeocystis Antarctica blooms strongly influence bacterial community structures in the Amundsen Sea polynya. *Front Microbiol* **5**: 1–13.

Delmont, T.O., Murat Eren, A., Vineis, J.H., and Post, A.F. (2015) Genome reconstructions indicate the partitioning of ecological functions inside a phytoplankton bloom in the Amundsen Sea, Antarctica. *Front Microbiol* **6**: 1–19.

Denef, V.J., Fujimoto, M., Berry, M.A., and Schmidt, M.L. (2016) Seasonal succession leads to habitat-dependent differentiation in ribosomal RNA:DNA ratios among freshwater lake bacteria. *Front Microbiol* **7**: 1–13.

Diepenbroek, M., Glöckner, F.O., Grobe, P., Güntsch, A., Huber, R., König-Ries, B., *et al*. (2014) Towards an integrated biodiversity and ecological research data management and archiving platform: the German federation for the curation of biological data (GFBio). In *Informatik 2014*, pp. 1711–1721.

Ducklow, H.W., Kirchman, D.L., Quinby, H.L., Carlson, C.A., and Dam, H.G. (1993) Stocks and dynamics of bacterioplankton carbon during the spring bloom in the eastern North Atlantic Ocean. *Deep Res Part II* **40**: 245–263.

Ducklow, H.W., Myers, K.M.S., Erickson, M., Ghiglione, J.F., and Murray, A.E. (2011) Response of a summertime Antarctic marine bacterial community to glucose and ammonium enrichment. *Aquat Microb Ecol* **64**: 205–220.

Ducklow, H.W., Schofield, O., Vernet, M., Stammerjohn, S., and Erickson, M. (2012) Multiscale control of bacterial production by phytoplankton dynamics and sea ice along the western Antarctic peninsula: a regional and decadal investigation. *J Mar Syst* **98–99**: 26–39.

Engel, A., Borchard, C., Piontek, J., Schulz, K.G., Riebesell, U., and Bellerby, R. (2013) CO_2 increases ^{14}C-primary production in an Arctic plankton community. *Biogeosciences* **10**: 1291–1308.

Engel, A., and Galgani, L. (2016) The organic sea-surface microlayer in the upwelling region off the coast of Peru and potential implications for air-sea exchange processes. *Biogeosciences* **13**: 989–1007.

Engel, A., Goldthwait, S., Passow, U., and Alldredge, A. (2002) Temporal decoupling of carbon and nitrogen dynamics in a mesocosm diatom bloom. *Limnol Oceanogr* **47**: 753–761.

Engel, A., and Händel, N. (2011) A novel protocol for determining the concentration and composition of sugars in particulate and in high molecular weight dissolved organic matter (HMW-DOM) in seawater. *Mar Chem* **127**: 180–191.

Frank, E., and Harrell, Jr. (2021) Hmisc: Harrell Miscellaneous. R package version 4.6-0. https://CRAN.R-project.org/package=Hmisc

Frölicher, T.L., Sarmiento, J.L., Paynter, D.J., Dunne, J.P., Krasting, J.P., and Winton, M. (2015) Dominance of the Southern Ocean in anthropogenic carbon and heat uptake in CMIP5 models. *J Clim* **28**: 862–886.

González, J.M., Fernández-Gómez, B., Fernàndez-Guerra, A., Gómez-Consarnau, L., Sánchez, O., Coll-

Lladó, M., *et al*. (2008) Genome analysis of the proteorhodopsin-containing marine bacterium Polaribacter sp. MED152 (Flavobacteria). *Proc Natl Acad Sci U S A* **105**: 8724–8729.

Granum, E., Kirkvold, S., and Myklestad, S.M. (2002) Cellular and extracellular production of carbohydrates and amino acids by the marine diatom Skeletonema costatum: diel variations and effects of N depletion. *Mar Ecol Prog Ser* **242**: 83–94.

Grasshoff, K., Ehrhardt, M., and Kremling, K. (1983) *Methods of Seawater Analysis*. New York: Verlag Chemie Weinhein, p. 419.

Grzymski, J.J., Riesenfeld, C.S., Williams, T.J., Dussaq, A. M., Ducklow, H., Erickson, M., *et al*. (2012) A metagenomic assessment of winter and summer bacterioplankton from Antarctica peninsula coastal surface waters. *ISME J* **6**: 1901–1915.

Henson, S.A., Sanders, R., and Madsen, E. (2012) Global patterns in efficiency of particulate organic carbon export and transfer to the deep ocean. *Global Biogeochem Cycles* **26**: 1–14.

Hsieh, T.C., Ma, K.H., and Anne, C. (2020) iNEXT: iNterpolation and EXTrapolation for species diversity. R package version 2.0.20 URL: http://chao.stat.nthu.edu.tw/wordpress/software-download/

Hoppema, M., Middag, R., De Baar, H.J.W., Fahrbach, E., Van Weerlee, E.M., and Thomas, H. (2007) Whole season net community production in the Weddell Sea. *Polar Biol* **31**: 101–111.

Imhoff, J.F., Rahn, T., Künzel, S., and Neulinger, S.C. (2018) Photosynthesis is widely distributed among Proteobacteria as demonstrated by the phylogeny of PufLM reaction center proteins. *Front Microbiol* **8**: 1–11.

Ingalls, A.E., Lee, C., Wakeham, S.G., and Hedges, J.I. (2003) The role of biominerals in the sinking flux and preservation of amino acids in the Southern Ocean along 170°W. *Deep Res Part II Top Stud Oceanogr* **50**: 713–738.

Janout, M.A., Hellmer, H.H., and Schröder, M. (2018) *Underway CTD Measurements During POLARSTERN Cruise PS111*. PANGAEA, Bremerhaven: Alfred Wegener Institute, Helmholtz Centre for Polar and Marine Research. https://doi.org/10.1594/PANGAEA895808.

Johnson, W.M., Alexander, H., Bier, R.L., Miller, D.R., Muscarella, M.E., Pitz, K.J., and Smith, H. (2020) Auxotrophic interactions: a stabilizing attribute of aquatic microbial communities? *FEMS Microbiol Ecol* **96**: 1–14.

Kähler, P., Björnsen, P.K., Lochte, K., and Antia, A. (1997) Dissolved organic matter and its utilization by bacteria during spring in the Southern Ocean. *Deep Res Part II Top Stud Oceanogr* **44**: 341–353.

Kaiser, K., and Benner, R. (2009) Biochemical composition and size distribution of organic matter at the Pacific and Atlantic time-series stations. *Mar Chem* **113**: 63–77.

Kappelmann, L., Krüger, K., Hehemann, J.H., Harder, J., Markert, S., Unfried, F., *et al*. (2019) Polysaccharide utilization loci of North Sea Flavobacteriia as basis for using SusC/D-protein expression for predicting major phytoplankton glycans. *ISME J* **13**: 76–91.

Kim, H., and Ducklow, H.W. (2016) A decadal (2002-2014) analysis for dynamics of heterotrophic bacteria in an Antarctic coastal ecosystem: variability and physical and biogeochemical forcings. *Front Mar Sci* **3**: 1–18.

Kirchman, D.L., Morán, X.A.G., and Ducklow, H. (2009) Microbial growth in the polar oceans – role of temperature and potential impact of climate change. *Nat Rev Microbiol* **7**: 451–459.

Kirchman, D.L., Rich, J.H., and Barber, R.T. (1995) Biomass and biomass production of heterotrophic bacteria along 140 degree W in the Equatorial Pacific: effect of temperature on the microbial loop. *Deep Res II* **42**: 603–619.

Lane, D. (1991) 16S/23S rRNA sequencing. In *Nucleic Acid Techniques in Bacterial Systematics*, Stackebrandt, E., and Goodfellow, M. (eds). Chichester, New York: Wiley.

Lechtenfeld, O.J., Kattner, G., Flerus, R., McCallister, S.L., Schmitt-Kopplin, P., and Koch, B.P. (2014) Molecular transformation and degradation of refractory dissolved organic matter in the Atlantic and Southern Ocean. *Geochim Cosmochim Acta* **126**: 321–337.

Lima-Mendez, G., Faust, K., Henry, N., Decelle, J., Colin, S., Carcillo, F., *et al*. (2015) Determinants of community structure in the grobal plankton interactome. *Science* **348**: 1262073.

Lindroth, P., and Mopper, K. (1979) High performance liquid chromatographic determination of subpicomole amounts of amino acids by precolumn fluorescence derivatization with o-phthaldialdehyde. *Anal Chem* **51**: 1667–1674.

Liu, Y., Blain, S., Crispi, O., Rembauville, M., and Obernosterer, I. (2020) Seasonal dynamics of prokaryotes and their associations with diatoms in the Southern Ocean as revealed by an autonomous sampler. *Environ Microbiol* **22**: 3968–3984.

Loginova, A.N., Thomsen, S., Dengler, M., Lüdke, J., and Engel, A. (2019) Diapycnal dissolved organic matter supply into the upper Peruvian oxycline. *Biogeosciences* **16**: 2033–2047.

Love, M.I., Huber, W., and Anders, S. (2014) Moderated estimation of fold change and dispersion for RNA-seq data with DESeq2. *Genome Biol* **15**: 1–21.

Luria, C.M., Amaral-Zettler, L.A., Ducklow, H.W., and Rich, J.J. (2016) Seasonal succession of free-living bacterial communities in coastal waters of the western antarctic peninsula. *Front Microbiol* **7**: 1–13.

Manna, V., Malfatti, F., Banchi, E., Cerino, F., De Pascale, F., Franzo, A., *et al*. (2020) Prokaryotic response to phytodetritus-derived organic material in epi- and mesopelagic Antarctic waters. *Front Microbiol* **11**: 1–18.

Massana, R., Taylor, L.T., Murray, A.E., Wu, K.Y., Jeffrey, W.H., and DeLong, E.F. (1998) Vertical distribution and temporal variation of marine planktonic archaea in the Gerlache Strait, Antarctica, during early spring. *Limnol Oceanogr* **43**: 607–617.

McMurdie, P.J., and Holmes, S. (2013) Phyloseq: an R package for reproducible interactive analysis and graphics of microbiome census data. *PLoS One* **8**: e61217.

Merbt, S.N., Stahl, D.A., Casamayor, E.O., Martí, E., Nicol, G.W., and Prosser, J.I. (2012) Differential photoinhibition of bacterial and archaeal ammonia oxidation. *FEMS Microbiol Lett* **327**: 41–46.

Morán, X.A.G., Sébastian, M., Pedrós-Alió, C., and Estrada, M. (2006) Response of Southern Ocean

phytoplankton and bacterioplankton production to short-term experimental warming. *Limnol Oceanogr* **51**: 1791–1800.

Morris, R.M., and Spietz, R.L. (2022) The physiology and biogeochemistry of SUP05. *Annu Rev Mar Sci* **14**: 1–15.

Murray, A.E., Wu, K.Y., Moyer, C.L., Karl, D.M., and DeLong, E.F. (1999) Evidence for circumpolar distribution of planktonic archaea in the Southern Ocean. *Aquat Microb Ecol* **18**: 263–273.

Newman, M.E.J. (2004) Fast algorithm for detecting community structure in networks. *Phys Rev E* **69**: 5.

Nguyen, R.T., and Harvey, H.R. (1997) Protein and amino acid cycling during phytoplankton decomposition in oxic and anoxic waters. *Org Geochem* **27**: 115–128.

Ogawa, H., Fukuda, R., and Koike, I. (1999) Vertical distributions of dissolved organic carbon and nitrogen in the Southern Ocean. *Deep Res Part I Oceanogr Res Pap* **46**: 1809–1826.

Oksanen, J., Blanchet, F.G., Friendly, M., Kindt, R., Legendre, P., and McGlinn, D. (2020) vegan: Community Ecology. R Package Version 2.5-7.

Olson, D.K., Yoshizawa, S., Boeuf, D., Iwasaki, W., and Delong, E.F. (2018) Proteorhodopsin variability and distribution in the North Pacific Subtropical Gyre. *ISME J* **12**: 1047–1060.

Parkinson, C.L. (2019) A 40-y record reveals gradual Antarctic Sea ice increases followed by decreases at rates far exceeding the rates seen in the Arctic. *Proc Natl Acad Sci U S A* **116**: 14414–14423.

Piontek, J., Galgani, L., Nöthig, E.M., Peeken, I., and Engel, A. (2021) Organic matter composition and heterotrophic bacterial activity at declining summer sea ice in the Central Arctic Ocean. *Limnol Oceanogr* **66**: S343–S362.

Pomeroy, L.R., and Deibel, D. (1986) Temperature regulation of bacterial activity during the spring bloom in newfoundland coastal waters. *Science* **233**: 359–361.

Qian, J., and Mopper, K. (1996) Automated high-performance, high-temperature combustion total organic carbon analyzer. *Anal Chem* **68**: 3090–3097.

Quast, C., Pruesse, E., Yilmaz, P., Gerken, J., Schweer, T., Yarza, P., *et al*. (2013) The SILVA ribosomal RNA gene database project: improved data processing and web-based tools. *Nucleic Acids Res* **41**: 590–596.

R Core Team. (2021) *R: A Language and Environment for Statistical Computing*. Vienna: Austria.

Redfield, A.C. (1958) No the biological control of chemical factors in the environment. *Am Sci* **46**: 205–221.

Riemann, B., Jørgensen, N.O.G., Lampert, W., and Fuhrman, J.A. (1986) Zooplankton induced changes in dissolved free amino acids and in production rates of freshwater bacteria. *Microb Ecol* **12**: 247–258.

Roller, B.R.K., and Schmidt, T.M. (2015) The physiology and ecological implications of efficient growth. *ISME J* **9**: 1481–1487.

RStudio Team. (2020) *RStudio: Integrated Development for R*. PBC, Boston, MA: RStudio.

Salazar, G., Paoli, L., Alberti, A., Huerta-Cepas, J., Ruscheweyh, H.J., Cuenca, M., *et al*. (2019) Gene expression changes and community turnover differentially shape the global ocean metatranscriptome. *Cell* **179**: 1068–1083.e21.

Schwieger, F., and Tebbe, C.C. (1998) A new approach to utilize PCR-single-strand-conformation polymorphism for 16S rRNA gene-based microbial community analysis. *Appl Environ Microbiol* **64**: 4870–4876.

Shen, Y., Benner, R., Murray, A.E., Gimpel, C., Mitchell, B. G., Weiss, E.L., and Reiss, C. (2017) Bioavailable dissolved organic matter and biological hot spots during austral winter in Antarctic waters. *J Geophys Res Ocean* **122**: 508–520.

Silvester, N., Alako, B., Amid, C., Cerdeño-Tarrága, A., Clarke, L., Cleland, I., *et al*. (2018) The European nucleotide archive in 2017. *Nucleic Acids Res* **46**: D36–D40.

Simon, M., and Azam, F. (1989) Protein content and protein synthesis rates of planktonic marine bacteria. *Mar Ecol Prog Ser* **51**: 201–213.

Sipler, R.E., and Connelly, T.L. (2015) Bioavailability of surface dissolved organic matter to aphotic bacterial communities in the Amundsen Sea Polynya, Antarctica. *Elementa* **3**: 1–13.

Smith, W.O., Dinniman, M.S., Klinck, J.M., and Hofmann, E. (2003) Biogeochemical climatologies in the Ross Sea, Antarctica: seasonal patterns of nutrients and biomass. *Deep Res Part II Top Stud Oceanogr* **50**: 3083–3101.

Song, H.J., Jung Kang, J., Kyung Kim, B., Joo, H.T., Jin Yang, E., Park, J., *et al*. (2016) High protein production of phytoplankton in the Amundsen Sea. *Deep Res Part II Top Stud Oceanogr* **123**: 50–57.

Sperling, M., Piontek, J., Engel, A., Wiltshire, K.H., Niggemann, J., Gerdts, G., *et al*. (2017) Combined carbohydrates support rich communities of particle-associated marine bacterioplankton. *Front Microbiol* **8**: 1–14.

Steven, B., Pollard, W.H., Greer, C.W., and Whyte, L.G. (2008) Microbial diversity and activity through a permafrost/ground ice core profile from the Canadian high Arctic. *Environ Microbiol* **10**: 3388–3403.

Sundberg, C., Al-Soud, W.A., Larsson, M., Alm, E., Yekta, S. S., Svensson, B.H., *et al*. (2013) 454 pyrosequencing analyses of bacterial and archaeal richness in 21 full-scale biogas digesters. *FEMS Microbiol Ecol* **85**: 612–626.

Trabelsi, A., and Rassoulzadegan, F. (2011) Effect of bacterial community dynamics on DOC seasonal changes in the north-western Mediterranean Sea. *J Plankton Res* **33**: 1249–1262.

Treusch, A.H., Vergin, K.L., Finlay, L.A., Donatz, M.G., Burton, R.M., Carlson, C.A., and Giovannoni, S.J. (2009) Seasonality and vertical structure of microbial communities in an ocean gyre. *ISME J* **3**: 1148–1163.

Tuorto, S.J., Darias, P., McGuinness, L.R., Panikov, N., Zhang, T., Häggblom, M.M., and Kerkhof, L.J. (2014) Bacterial genome replication at subzero temperatures in permafrost. *ISME J* **8**: 139–149.

Turner, J., Guarino, M.V., Arnatt, J., Jena, B., Marshall, G.J., Phillips, T., *et al*. (2020) Recent decrease of summer sea ice in the Weddell Sea, Antarctica. *Geophys Res Lett* **47**: e2020GL087127.

van Vliet, D.M., von Meijenfeldt, F.A.B., Dutilh, B.E., Villanueva, L., Sinninghe Damsté, J.S., Stams, A.J.M., and Sánchez-Andrea, I. (2021) The bacterial sulfur cycle in expanding dysoxic and euxinic marine waters. *Environ Microbiol* **23**: 2834–2857.

von Bröckel, K. (1985) Primary production data from the South-Eastern Weddell Sea. *Polar Biol* **4**: 75–80.

Von Jackowski, A., Grosse, J., Nöthig, E.M., and Engel, A. (2020) Dynamics of organic matter and bacterial activity in the Fram Strait during summer and autumn: DOM and bacteria in Fram Strait. *Philos Trans R Soc A Math Phys Eng Sci* **378**: 20190366.

Welschmeyer, N.A. (1994) Fluorometric analysis of chlorophyll a in the presence of chlorophyll b and pheopigments. *Limnol Oceanogr* **39**: 1985–1992.

Wiebinga, C.J., and De Baar, H.J.W. (1998) Determination of the distribution of dissolved organic carbon in the Indian sector of the Southern Ocean. *Mar Chem* **61**: 185–201.

Williams, C.M., Dupont, A.M., Loevenich, J., Post, A.F., Dinasquet, J., and Yager, P.L. (2016) Pelagic microbial heterotrophy in response to a highly productive bloom of Phaeocystis Antarctica in the Amundsen Sea Polynya, Antarctica. *Elem Sci Anthr* **2016**: 1–18.

Yager, P., Sherrell, R., Stammerjohn, S., Ducklow, H., Schofield, O., Ingall, E., *et al*. (2016) A carbon budget for the Amundsen Sea Polynya, Antarctica: estimating net community production and export in a highly productive polar ecosystem. *Elem Sci Anthr* **4**: 1–36.

Supporting Information

Additional Supporting Information may be found in the online version of this article at the publisher's web-site:

Appendix S1. Supporting Information.

Table S1. Chlorophyll a (Chl-a) concentration, net community production (NCP) and nutrient depletion ratios. The means and standard deviations are reported.

Table S2. Composition (mol%) of dissolved amino acids. The means and standard deviations for the different depth intervals at Bloom stations and Low-Chl stations are reported.

Table S3. Composition (mol%) of dissolved combined carbohydrates. The means and standard deviations for the different depth intervals at Bloom stations and Low-Chl stations are reported.

Table S4. Indices of alpha-diversity for 16S rRNA gene sequences and 16S rRNA sequences at Bloom stations and Low-chlorophyll (Low-Chl) stations. Differences between the upper mixed layer and waters below the pycnocline at both groups of stations were tested in a two-way ANOVA.

Fig. S1. Seasonal sea-ice dynamics and chlorophyll a concentrations derived from remote-sensing observations at (A) the Ronne Polynya and (B) the Halley Bay Polynya. Sea ice data were downloaded from www.meereisportal.de, and chlorophyll-*a* data from www.oceancolour.org.

Fig. S2. Major classes in Weddell Sea bacterioplankton. Composition of the 16S rRNA sequences. Stations are ordered according to their chlorophyll a concentration, from highest (station 28) to lowest (station 47). Classes with median proportions ≥1% (across all samples) are shown individually, and those with proportions <1% are summarized within the category Other Classes. *Alphaproteobacteria* were further split into the *Roseobacter* clade, the SAR11 clade, and other groups.

Fig. S3. Venn diagram. The numbers of shared and unique amplicon sequence variants (ASVs) at Bloom stations, Low-Chl stations, and the northern stations at Maud Rise (N).

Fig. S4. DESeq2 analysis of differentially abundant ASVs at stations with strongly diatom-dominated phytoplankton and at *Phaeocystis*-rich stations. ASVs with significantly larger shares at diatom-dominated stations (log2-fold change <0) are indicated by squares, and those with significantly higher proportions at stations with elevated shares of *Phaeocystis* sp. (log2-fold change >0) by circles. The highlighted ASVs 1, 17 and 44 were among the 20 most abundant sequence variants in the data set (average sequence proportions across all samples 21%, 1.7%, 1.0% respectively).

Fig. S5. Depth profiles of the 20 most abundant amplicon sequence variants (ASVs) in surface waters at Bloom stations, Low-Chl stations, and northern stations at Maud Rise (64.0–66.7°S) (N). Abundance was estimated by multiplying the percentage of 16S rRNA gene reads by the total prokaryotic cell number. ASVs with a significantly higher abundance at Bloom stations than at Low-Chl stations, as inferred from a DESeq2 analysis. (A) ASVs with significantly higher abundance at Bloom stations than at Low-Chl stations, as inferred from a DESeq2 analysis. (B) ASVs without significant differences in abundance between Bloom stations and Low-Chl stations, as inferred from a DESeq2 analysis. ASVs with significantly higher abundance at Low-Chl stations than at Bloom stations, as inferred from a DESeq2 analysis.

Fig. S6. Abundance of (A) bacteria and (B) nanoflagellates at Bloom stations, Low-Chl stations, and northern stations at Maud Rise (64.0–66.7°S) (N). Lines trace the mean values of Bloom stations and Low-Chl stations, with shaded areas representing the 95% confidence intervals. Closed circles denote strongly diatom-dominated stations, and open circles stations with higher contributions of *Phaeocystis* sp.

Table S5. Closest relatives of the 20 most abundant Weddell Sea amplicon sequence variants in GenBank.

All GenBank entries included in peer-reviewed publications were considered. All entries with 100% sequence identity are included (April 2021). In case of less than three 100% similar sequences, the three hits with the highest similarities were listed.